Eur. Phys. J. C (2024) 84:1329
https://doi.org/10.1140/epjc/s10052-024-13666-w

THE EUROPEAN PHYSICAL JOURNAL C

Regular Article - Theoretical Physics

Leptonic dipole operator with Γ_2 modular invariance in light of Muon $(g-2)_\mu$

Takaaki Nomura[1,a], **Morimitsu Tanimoto**[2,b], **Xing-Yu Wang**[1,c]

[1] College of Physics, Sichuan University, Chengdu 610065, China
[2] Department of Physics, Niigata University, Niigata 950-2181, Japan

Received: 14 October 2024 / Accepted: 28 November 2024

Abstract We have studied the leptonic EDM and the LFV decays relating with the recent data of anomalous magnetic moment of muon, $(g-2)_\mu$ in the leptonic dipole operator. We have adopted the successful Γ_2 modular invariant model by Meloni–Parriciatu as the flavor symmetry of leptons. Suppose the anomaly of $(g-2)_\mu$, Δa_μ to be evidence of New Physics (NP), we have related it with the anomalous magnetic moment of the electron Δa_e, the electron EDM d_e and the $\mu \to e\gamma$ decay. We found that the NP contributions to $\Delta a_{e(\mu)}$ are proportional to the lepton masses squared likewise the naive scaling $\Delta a_\ell \propto m_\ell^2$. The experimental constraint of $|d_e|$ is much tight compared with the one from the branching ratio $\mathcal{B}(\mu \to e\gamma)$ in our framework. Supposing the phase of our model parameter δ_α for the electron to be of order one, we have estimated the upper-bound of $\mathcal{B}(\mu \to e\gamma)$, which is at most $10^{-21} - 10^{-20}$. If some model parameters are real, leptonic EDMs vanish since the CP phase of the modular form due to modulus τ does not contribute to the EDM. However, we can obtain $\mathcal{B}(\mu \to e\gamma) \simeq 10^{-13}$ with non-vanishing d_e in a specific case. The imaginary part of a parameter can lead to d_e in the next-to-leading contribution. The predicted electron EDM is below 10^{-32}e cm, while $\mathcal{B}(\mu \to e\gamma)$ is close to the experimental upper-bound. The branching ratios of $\tau \to e\gamma$ and $\tau \to \mu\gamma$ are also discussed.

1 Introduction

The electric and magnetic dipole moments of the charged leptons are low-energy probes of New Physics (NP) beyond the Standard Model (SM). The muon $(g-2)_\mu$ experiment at Fermilab reported a new measurement of the muon magnetic anomaly [1]. Improvements of the analysis and run condition lead to more than a factor of two reduction in the systematic uncertainties, which is compared with the E989 experiment at Fermilab [2] and the previous BNL result [3]. This result indicates the discrepancy of 5.1 σ with the SM prediction [4] (see also [5–14]).

While there is a debatable point on the precise value of the SM prediction, that is the contribution of the hadronic vacuum polarization (HVP). The current situation is still complicated. The CMD-3 collaboration [15] released results on the cross section that disagree at the $(2.5-5)\sigma$ level with all previous measurements. The origin of this discrepancy is currently unknown. The Bell-II experiment is expected to measure $e^+e^- \to \pi^+\pi^-$ cross section in the near future.[1] The BMW collaboration published the first complete lattice-QCD result with subpercent precision [17]. Their result is closer to the experimental average (1.7σ tension for no NP in the muon $(g-2)_\mu$). Further studies are underway to clarify these theoretical differences.

If the muon $(g-2)_\mu$ anomaly comes from NP, it possibly appears in other observables of the charged lepton sector. The interesting one is the electric dipole moments (EDM) of the electron. A new upper-bound on the electron EDM, which is $|d_e| < 4.1 \times 10^{-30}$e cm (90% confidence), was reported by the JILA group [18]. It overcame the latest ACME collaboration result obtained in 2018 [19]. Precise measurements of the electron EDM will be rapidly being updated. The future sensitivity at ACME III is expected to be $|d_e| < 0.3 \times 10^{-30}$ e cm [20,21]. On the other hand, the present upper-bound of the muon EDM [22] and tauon EDM [23–25] are not so tight.

[a] e-mail: nomura@scu.edu.cn
[b] e-mail: tanimoto@muse.sc.niigata-u.ac.jp
[c] e-mail: xingyuwang@stu.scu.edu.cn (corresponding author)

[1] Belle-II reported the measurement of the $e^+e^- \to \pi^+\pi^-\pi^0$ cross section in the energy range $0.62 - 3.50$ GeV. The result differs by 2.5 standard deviations from the most precise current determination [16].

Published online: 29 December 2024

The lepton flavor violation (LFV) is also possible NP phenomena of charged leptons. The tightest constraint for LFV is the branching ratio of the $\mu \to e\gamma$ decay. The recent experimental upper-bound is $\mathcal{B}(\mu^+ \to e^+\gamma) < 3.1 \times 10^{-13}$ by the combination of the MEG and MEG II experiments [26,27]. In contrast, the present upper-bounds of $\mathcal{B}(\tau \to \mu\gamma)$ and $\mathcal{B}(\tau \to e\gamma)$ are not so tight such as 4.4×10^{-8} and 3.3×10^{-8} [28,29], respectively.

On the other hand, theoretical studies of the electric and magnetic dipole moments of leptons are given in the SM Effective Field Theory (SMEFT) [30–32], i.e., under the hypothesis of new degrees of freedom above the electroweak scale [33–36]. The phenomenological discussion of NP has presented taking the anomaly of the muon $(g-2)_\mu$ and the LFV bound in the SMEFT. The flavor symmetry is a challenging hypothesis to reduce the number of independent parameters of the flavor sector. Indeed, LFV decays and the electron EDM have been studied in the light of the muon $(g-2)_\mu$ anomaly by imposing $U(2)_L \otimes U(2)_R$ flavor symmetry [37,38] and some other symmetries [39].

Recently, the modular invariance opened up a new promising approach to the flavor problem of quarks and leptons [40] (see also Refs. [41–43]). Among finite Γ_N modular groups, the Γ_3 modular group, which is isomorphic to A_4 [44–50], has been extensively used for understanding the origin of the quark and lepton flavors [40,51–65]. Other finite modular groups have been also widely employed in flavor model building (see, e.g., [41–43,66–77] and the reviews [78–89]). Furthermore, the modular symmetry is also developing to the strong CP problem [90–94] and modular inflation [95–98]. It is also remarked that the formalism of non-holomorphic modular flavor symmetry is developed [99].

In the framework of the A_4 modular flavor symmetry, LFV decays and the electron EDM have been studied with the muon $(g-2)_\mu$ anomaly [62,63]. In those works, assuming NP to be heavy and given by the SMEFT Lagrangian, the dipole operator of leptons and their Wilson coefficients were discussed at the electroweak scale. Although modular flavor models have been constructed in the supersymmetric framework so far, the modular invariant SMEFT will be realized in the so-called moduli-mediated supersymmetry breaking scenario [100]. Furthermore, higher-dimensional operators also keep the modular invariance in a certain class of the string effective field theory in which n-point couplings of matter fields are written by a product of 3-point couplings [101]. This is called *Stringy Ansatz* to constrain the higher-dimensional operators in the SMEFT.

In this work, we take the level 2 finite modular group, Γ_2 [41], which is isomorphic to the S_3 group, as the flavor symmetry. In the S_3 group, irreducible representations are two different singlets $\mathbf{1}, \mathbf{1}'$ and one doublet $\mathbf{2}$, which are assigned to quarks or leptons. Similarly, the light two families are assigned to $\mathbf{2}$ and the third one is $\mathbf{1}$ in the $U(2)$ flavor model. The $U(2)$ flavor symmetry is successful in the quark sector such as B meson physics [102,103]. On the other hand, the drawback of the $U(2)$ leptonic flavor model is in the difficulty of building a simple neutrino mass matrix. Therefore, the neutrino mass matrix is not specified in the analysis of the LFV decays and the electron EDM by imposing $U(2)$ in Refs. [37,38]. In the S_3 flavor model, simple lepton mass matrices possibly reproduce the masses and neutrino mixing angles under the Γ_2 modular invariance, where the modular symmetry and CP symmetry are broken by fixing the vacuum expectation value (VEV) of modulus τ. Indeed, the successful models of leptons have been presented [76,77]. Based on these works, we investigate LFV decays and the electron EDM relating with the muon $(g-2)_\mu$ anomaly.

The paper is organized as follows. In Sect. 2, we present our framework, that is *Stringy Ansatz* and the level 2 modular group. In Sect. 3, we show the flavor structure of the Wilson coefficients of the leptonic dipole operator in mass basis with input data. In Sect. 4, the Γ_2 modular invariant models of leptons are introduced. In Sect. 5, the Wilson coefficients are obtained approximately in mass basis. In Sect. 6, we discuss the phenomenology of the electron $(g-2)_e$, LFV decays and the electron EDM numerically. Section 7 is devoted to the summary. In Appendix A, we present the tensor product of the S_3 group. In Appendix B, we present the experimental constraints on the leptonic dipole operator. In Appendix C and D, we derive the left-handed and right-handed mixing matrices. In Appendix E, model parameters are discussed in the normal distribution.

2 Framework

2.1 Stringy ansatz

It was known that n-point couplings $y^{(n)}$ of matter fields are written by products of 3-point couplings $y^{(3)}$ in a certain class of string compactifications. For instance, 4-point couplings $y^{(4)}_{ijk\ell}$ of matter fields are given by

$$y^{(4)}_{ijk\ell} = \sum_m y^{(3)}_{ijm} y^{(3)}_{mk\ell}, \tag{1}$$

up to an overall factor where the subscripts "$\{i, j, k, \ell\}$" indicate states associated with corresponding 4-point interaction [101]. Here, the virtual modes "m" are light or heavy modes, depending on the compactifications. It indicates that the flavor structure of 3-point couplings and higher-dimensional operators has a common origin in string compactifications. As discussed in Ref. [101], such a relation holds at the low-energy scale below the compactification scale.

Indeed, the Ansatz Eq. (1) is used to predict NP of leptonic phenomena in the modular flavor symmetry, as will be discussed in the next sections.

2.2 Modular forms of Γ_2 modular group

The Γ_2 modular group is isomorphic to S_3 [41], where the irreducible representations are

$$\mathbf{1}, \quad \mathbf{1}', \quad \mathbf{2}. \tag{2}$$

These tensor products are given in Appendix A. By using the Dedekind eta-function $\eta(\tau)$:

$$\eta(\tau) = q^{1/24}\prod_{n=1}^{\infty}(1-q^n), \qquad q = e^{2\pi i\tau}, \tag{3}$$

the modular forms of weight 2 corresponding to the S_3 doublet are given as [41],

$$\mathbf{Y_2^{(2)}} = \begin{pmatrix} Y_1(\tau) \\ Y_2(\tau) \end{pmatrix}, \tag{4}$$

where

$$\begin{aligned} Y_1(\tau) &= \frac{1}{2}c\left(\frac{\eta'(\tau/2)}{\eta(\tau/2)} + \frac{\eta'((\tau+1)/2)}{\eta((\tau+1)/2)} - \frac{8\eta'(2\tau)}{\eta(2\tau)}\right), \\ Y_2(\tau) &= \frac{\sqrt{3}}{2}c\left(\frac{\eta'(\tau/2)}{\eta(\tau/2)} - \frac{\eta'((\tau+1)/2)}{\eta((\tau+1)/2)}\right). \end{aligned} \tag{5}$$

Here τ is the complex modulus. In these expressions, c is a normalization constant. The S_3 generators S and T are in the doublet representation:

$$S = \frac{1}{2}\begin{pmatrix} -1 & -\sqrt{3} \\ -\sqrt{3} & 1 \end{pmatrix}, \qquad T = \begin{pmatrix} 1 & 0 \\ 0 & -1 \end{pmatrix}. \tag{6}$$

Taking c as [76]:

$$c = i\frac{7}{25\pi}, \tag{7}$$

the doublet modular forms of weight 2 have the following q-expansions:

$$\mathbf{Y_2^{(2)}} = \begin{pmatrix} Y_1(\tau) \\ Y_2(\tau) \end{pmatrix} \simeq \begin{pmatrix} \frac{7}{100}(1+24q+24q^2+96q^3+\dots) \\ \frac{14}{25}\sqrt{3}q^{1/2}(1+4q+6q^2+\dots) \end{pmatrix}. \tag{8}$$

In the basis of Eq. (6), we can construct modular forms of weight 4 by the tensor product of the two doublets $(Y_1(\tau), Y_2(\tau))^T$:

$$\begin{aligned} \mathbf{1} &: \ \mathbf{Y_1^{(4)}} = Y_1(\tau)^2 + Y_2(\tau)^2, \\ \mathbf{2} &: \ \mathbf{Y_2^{(4)}} = \begin{pmatrix} Y_1^{(4)} \\ Y_2^{(4)} \end{pmatrix} = \begin{pmatrix} Y_2(\tau)^2 - Y_1(\tau)^2 \\ 2Y_1(\tau)Y_2(\tau) \end{pmatrix}. \end{aligned} \tag{9}$$

The S_3 singlet $\mathbf{1}'$ modular form of the weight 4 vanishes.

Likewise, we obtain the modular forms of weight 6 by tensor products of three modular forms with weight 2 as:

$$\begin{aligned} \mathbf{1} &: \ \mathbf{Y_1^{(6)}} = 3Y_1(\tau)Y_2(\tau)^2 - Y_1(\tau)^3, \\ \mathbf{1}' &: \ \mathbf{Y_{1'}^{(6)}} = Y_2(\tau)^3 - 3Y_1(\tau)^2Y_2(\tau), \\ \mathbf{2} &: \ \mathbf{Y_2^{(6)}} = \begin{pmatrix} Y_1^{(6)} \\ Y_2^{(6)} \end{pmatrix} = \begin{pmatrix} Y_1(\tau)(Y_1(\tau)^2 + Y_2(\tau)^2) \\ Y_2(\tau)(Y_1(\tau)^2 + Y_2(\tau)^2) \end{pmatrix}. \end{aligned} \tag{10}$$

In the case of the large Im τ, the modular forms of Y_1 and Y_2 are given by q expansions in good approximation. By using small parameter ϵ, the modular forms are written up to $\mathcal{O}(\epsilon)$ as:

$$\mathbf{Y_2^{(2)}} = \begin{pmatrix} Y_1(\tau) \\ Y_2(\tau) \end{pmatrix} \simeq \frac{7}{100}\begin{pmatrix} 1+24\epsilon p \\ 8\sqrt{3}\sqrt{\epsilon}p'(1+4\epsilon p) \end{pmatrix}, \tag{11}$$

where

$$\begin{aligned} &\epsilon = \exp[-2\pi \,\mathrm{Im}\,\tau], \qquad p = \exp[2\pi i\,\mathrm{Re}\,\tau], \\ &p' = \exp[\pi i\,\mathrm{Re}\,\tau]. \end{aligned} \tag{12}$$

Modular forms of weight 4 and 6 are written in terms of ϵ, p and p' as:

$$\begin{aligned} \mathbf{Y_1^{(4)}} &\simeq \left(\frac{7}{100}\right)^2(1+240\epsilon p), \\ Y_1^{(4)} &\simeq \left(\frac{7}{100}\right)^2(-1+144\epsilon p), \\ Y_2^{(4)} &\simeq \left(\frac{7}{100}\right)^2(16\sqrt{3}\sqrt{\epsilon}p'), \\ \mathbf{Y_1^{(6)}} &\simeq \left(\frac{7}{100}\right)^3(-1+504\epsilon p), \\ \mathbf{Y_{1'}^{(6)}} &\simeq \left(\frac{7}{100}\right)^3(-24\sqrt{3}\sqrt{\epsilon}p'), \\ Y_1^{(6)} &\simeq \left(\frac{7}{100}\right)^3(1+264\epsilon p), \\ Y_2^{(6)} &\simeq \left(\frac{7}{100}\right)^3(8\sqrt{3}\sqrt{\epsilon}p'). \end{aligned} \tag{13}$$

3 Constraints of Wilson coefficients of dipole operator

3.1 Input experimental data

The combined result from the E989 experiment at Fermilab [1,2] and the E821 experiment at BNL [3] on $a_\mu = (g-2)_\mu/2$, together with the SM prediction $a_\mu^{\rm SM}$ in [4], implies

$$\Delta a_\mu = a_\mu^{\rm Exp} - a_\mu^{\rm SM} = (249 \pm 49) \times 10^{-11}\,. \tag{14}$$

We suppose that Δa_μ comes from NP.

Although the precise value of the SM prediction of HVP is still unclear, we take a following reference value (the discrepancy of 5.1 σ with the SM prediction) as the input in our numerical analysis:

$$\Delta a_\mu = 249 \times 10^{-11}. \tag{15}$$

We also impose the upper-bound of the absolute value of electron EDM by the JILA group [18]:

$$|d_e| < 4.1 \times 10^{-30}\,\mathrm{e\,cm} = 6.3 \times 10^{-14}\,\mathrm{TeV}^{-1}. \tag{16}$$

On the other hand, the upper-bound of the muon EDM is [22]:

$$|d_\mu| < 1.8 \times 10^{-19}\,\mathrm{e\,cm} = 2.76 \times 10^{-3}\,\mathrm{TeV}^{-1}. \tag{17}$$

The tauon EDM can be evaluated through the measurement of CP-violating correlations in tauon-pair production such as $e^+e^- \to \tau^+\tau^-$ [23] (see also [24]). The present upper-bound on the tauon EDM d_τ is given as [25]:

$$\begin{aligned} &-1.85 \times 10^{-17}\mathrm{e\,cm} < \mathrm{Re}\, d_\tau < 0.61 \times 10^{-17}\mathrm{e\,cm}, \\ &-1.03 \times 10^{-17}\mathrm{e\,cm} < \mathrm{Im}\, d_\tau < 0.23 \times 10^{-17}\mathrm{e\,cm}. \end{aligned} \tag{18}$$

Taking the bound of $\mathrm{Re}\, d_\tau$, we have

$$|d_\tau| < 1.85 \times 10^{-17}\mathrm{e\,cm} = 2.84 \times 10^{-1}\,\mathrm{TeV}^{-1}. \tag{19}$$

The experimental upper-bound for the branching ratio of the $\mu \to e\gamma$ decay is [26,27]:

$$\mathcal{B}(\mu^+ \to e^+\gamma) < 3.1 \times 10^{-13}. \tag{20}$$

We also take account of the upper-bound for LFV decays $\tau \to \mu\gamma$ and $\tau \to e\gamma$ [28,29]:

$$\mathcal{B}(\tau \to \mu\gamma) < 4.2 \times 10^{-8}, \quad \mathcal{B}(\tau \to e\gamma) < 3.3 \times 10^{-8}. \tag{21}$$

These input data are summarized in Table 1. They are converted into the magnitudes of the Wilson coefficients of the leptonic dipole operator in the next subsection.

3.2 Wilson coefficients of leptonic dipole operator

We make the assumption that NP is heavy and can be given by the SMEFT Lagrangian. Let us focus on the dipole operator of leptons and their Wilson coefficients. The dipole operators come from SMEFT Lagrangian at the weak scale as:

$$\begin{aligned} &\mathcal{O}_{\substack{e\gamma \\ RL}} = \frac{v}{\sqrt{2}}\overline{E}_R\sigma^{\mu\nu}E_L F_{\mu\nu}, \qquad \mathcal{C}'_{\substack{e\gamma \\ RL}} = \begin{pmatrix} \mathcal{C}'_{\substack{e\gamma \\ ee}} & \mathcal{C}'_{\substack{e\gamma \\ e\mu}} & \mathcal{C}'_{\substack{e\gamma \\ e\tau}} \\ \mathcal{C}'_{\substack{e\gamma \\ \mu e}} & \mathcal{C}'_{\substack{e\gamma \\ \mu\mu}} & \mathcal{C}'_{\substack{e\gamma \\ \mu\tau}} \\ \mathcal{C}'_{\substack{e\gamma \\ \tau e}} & \mathcal{C}'_{\substack{e\gamma \\ \tau\mu}} & \mathcal{C}'_{\substack{e\gamma \\ \tau\tau}} \end{pmatrix}, \\ &\mathcal{O}_{\substack{e\gamma \\ LR}} = \frac{v}{\sqrt{2}}\overline{E}_L\sigma^{\mu\nu}E_R F_{\mu\nu}, \qquad \mathcal{C}'_{\substack{e\gamma \\ LR}} = \mathcal{C}'^{\dagger}_{\substack{e\gamma \\ RL}}, \end{aligned} \tag{22}$$

where E_L and E_R denote three flavors of the left-handed and right-handed charged leptons, respectively, and v denotes the vacuum expectation value (VEV) of the Higgs field H. The prime of the Wilson coefficients indicates the mass-eigenstate basis of the charged leptons. (Later, we use the notation of the Wilson coefficients without primes in the basis of the non-diagonal charged lepton mass matrix.) The relevant effective Lagrangian is written as:

$$\mathcal{L}_{\mathrm{dipole}} = \frac{1}{\Lambda^2}\left(\mathcal{C}'_{\substack{e\gamma \\ RL}}\mathcal{O}_{\substack{e\gamma \\ RL}} + \mathcal{C}'_{\substack{e\gamma \\ LR}}\mathcal{O}_{\substack{e\gamma \\ LR}}\right), \tag{23}$$

where Λ is a certain mass scale of NP in the effective theory.

The operator of Eq. (22) corresponds to the four-field operator of SMEFT $[\overline{E}_R\sigma^{\mu\nu}E_L H F_{\mu\nu}]$ by replacing v with H. In the viewpoint of *Stringy Ansatz* of Eq. (1), the lightest mode "m" corresponds to the Higgs doublet. If the mode "m" is only Higgs doublet, the flavor structure of bilinear operator $[\,\bar{E}_R\sigma^{\mu\nu}E_L\,]$ is exactly the same as the mass matrix. Obviously, the bilinear operator matrix is diagonal in the basis for mass eigenstates. In this case the LFV processes such as $\mu \to e$, $\tau \to \mu$ and $\tau \to e$ never happen.

However, additional unknown modes "m" in Eq. (1) can cause the flavor violation. We discuss such a case in our numerical analysis.

In the following discussions, we take the Γ_2 modular symmetry for leptons. Most of modular flavor models are supersymmetric models. Since we discuss the model below the supersymmetry breaking scale, the light modes are exactly the same as the SM with two Higgs doublet models. Note that the modular symmetry is still a symmetry of the low-energy effective action below the supersymmetry breaking scale, as confirmed in the moduli-mediated supersymmetry breaking scenario [100]. Here the Wilson coefficients are understood to be evaluated at the weak scale.[2] Inputting the value in Eq. (15), the $\mu\mu$ component of Wilson coefficients is obtained as [37] (see Appendix B):

$$\frac{1}{\Lambda^2}\mathrm{Re}\,[\mathcal{C}'_{\substack{e\gamma \\ \mu\mu}}] = 1.0 \times 10^{-5}\,\mathrm{TeV}^{-2}. \tag{24}$$

[2] We neglect the small effect of running below the weak scale. The one-loop effect is small as seen in [104].

Table 1 Relevant observables and the corresponding values of Wilson coefficients, which are presented in $1/\Lambda^2$ (TeV^{-2}) unit

Observables	Exp.-SM/upper bound	Wilson Coef. in $1/\Lambda^2$ (TeV^{-2})
Δa_μ	249×10^{-11} [1–3]	Re $[\mathcal{C}'_{\substack{e\gamma \\ \mu\mu}}] = 1.0 \times 10^{-5}$
$\mathcal{B}(\mu^+ \to e^+\gamma)$	$< 3.1 \times 10^{-13}$ [26]	$\lvert\mathcal{C}'_{\substack{e\gamma \\ e\mu(\mu e)}}\rvert < 1.8 \times 10^{-10}$
$\mathcal{B}(\tau \to \mu\gamma)$	$< 4.2 \times 10^{-8}$ [28,29]	$\lvert\mathcal{C}'_{\substack{e\gamma \\ \mu\tau(\tau\mu)}}\rvert < 2.65 \times 10^{-6}$
$\mathcal{B}(\tau \to e\gamma)$	$< 3.3 \times 10^{-8}$ [28,29]	$\lvert\mathcal{C}'_{\substack{e\gamma \\ e\tau(\tau e)}}\rvert < 2.35 \times 10^{-6}$
$\lvert d_e \rvert$	$< 4.1 \times 10^{-30}$ e cm [18]	Im $[\mathcal{C}'_{\substack{e\gamma \\ ee}}] < 1.8 \times 10^{-13}$
$\lvert d_\mu \rvert$	$< 1.80 \times 10^{-19}$ e cm [22]	Im $[\mathcal{C}'_{\substack{e\gamma \\ \mu\mu}}] < 7.9 \times 10^{-3}$
$\lvert d_\tau \rvert$	$< 1.85 \times 10^{-17}$ e cm [23]	Im $[\mathcal{C}'_{\substack{e\gamma \\ \tau\tau}}] < 8.2 \times 10^{-1}$

The LFV process $\mu \to e\gamma$ gives us more severe constraint for the $\mu e(e\mu)$ component of Wilson coefficients by the experimental data in Eq. (20). The upper-bound is obtained [37] (see Appendix B):

$$\frac{1}{\Lambda^2}\lvert\mathcal{C}'_{\substack{e\gamma \\ e\mu(\mu e)}}\rvert < 1.8 \times 10^{-10}\,\text{TeV}^{-2}. \tag{25}$$

Taking into account Eqs. (24) and (25), one has the ratio [37]:

$$\left|\frac{\mathcal{C}'_{\substack{e\gamma \\ e\mu(\mu e)}}}{\mathcal{C}'_{\substack{e\gamma \\ \mu\mu}}}\right| < 1.8 \times 10^{-5}. \tag{26}$$

Thus, the magnitude of $\mathcal{C}'_{\substack{e\gamma \\ e\mu(\mu e)}}$ is much suppressed compared with $\mathcal{C}'_{\substack{e\gamma \\ \mu\mu}}$. This gives the severe constraint for parameters of the flavor model.

The $\tau \to e\gamma$ and $\tau \to \mu\gamma$ decays also give us constraints by the experimental data in Eq. (21). The upper-bounds of corresponding components of the Wilson coefficients are obtained as seen in Appendix B:

$$\begin{aligned}\frac{1}{\Lambda^2}\lvert\mathcal{C}'_{\substack{e\gamma \\ \mu\tau(\tau\mu)}}\rvert &< 2.65 \times 10^{-6}\,\text{TeV}^{-2}, \\ \frac{1}{\Lambda^2}\lvert\mathcal{C}'_{\substack{e\gamma \\ e\tau(\tau e)}}\rvert &< 2.35 \times 10^{-6}\,\text{TeV}^{-2}.\end{aligned} \tag{27}$$

The electron EDM, d_e is defined in the operator:

$$\mathcal{O}_{\text{edm}} = -\frac{i}{2}\, d_e(\mu)\, \bar{e}\sigma^{\mu\nu}\gamma_5 e F_{\mu\nu}, \tag{28}$$

where $d_e = d_e(\mu = m_e)$. Therefore, the electron EDM is extracted from the effective Lagrangian

$$\mathcal{L}_{\text{EDM}} = \frac{1}{\Lambda^2}\mathcal{C}'_{\substack{e\gamma \\ ee}}\mathcal{O}_{\substack{e\gamma \\ LR}} + \text{h.c.} = \frac{1}{\Lambda^2}\mathcal{C}'_{\substack{e\gamma \\ ee}}\frac{v}{\sqrt{2}}\bar{e}_L\sigma^{\mu\nu}e_R F_{\mu\nu} + \text{h.c.}, \tag{29}$$

which leads to

$$d_e = -\sqrt{2}\,\frac{v}{\Lambda^2}\,\text{Im}\,[\mathcal{C}'_{\substack{e\gamma \\ ee}}], \tag{30}$$

at tree level, where the small effect of running below the electroweak scale is neglected.

Inputting the experimental upper-bound of the electron EDM in Eq. (16) [18], we obtain ee component of the constraints of the Wilson coefficient:

$$\frac{1}{\Lambda^2}\text{Im}\,[\mathcal{C}'_{\substack{e\gamma \\ ee}}] < 1.8 \times 10^{-13}\,\text{TeV}^{-2}. \tag{31}$$

By taking the value in Eq. (24), we have a very small ratio:

$$\frac{\text{Im}\,[\mathcal{C}'_{\substack{e\gamma \\ e\mu(\mu e)}}]}{\text{Re}\,[\mathcal{C}'_{\substack{e\gamma \\ \mu\mu}}]} < 1.8 \times 10^{-8}. \tag{32}$$

On the other hand, the experimental upper-bound of the muon EDM in Eq. (17) gives:

$$\frac{1}{\Lambda^2}\text{Im}\,[\mathcal{C}'_{\substack{e\gamma \\ \mu\mu}}] < 7.9 \times 10^{-3}\,\text{TeV}^{-2}. \tag{33}$$

The upper-bound of the tauon EDM in Eq. (19) also gives:

$$\frac{1}{\Lambda^2}\text{Im}\,[\mathcal{C}'_{\substack{e\gamma \\ \tau\tau}}] < 8.2 \times 10^{-1}\,\text{TeV}^{-2}. \tag{34}$$

These upper-bounds of the Wilson coefficients are summarized in Table 1. Using these upper-bounds of Wilson coefficients, we discuss NP based on the Γ_2 modular invariant flavor model in the next section.

Table 2 Assignments of S_3 representations and weights in Model I

	$(e,\mu)_L$, τ_L	e^c, μ^c, τ^c	H_u	H_d
$SU(2)$	2	1	2	2
S_3	2 $1'$	1 $1'$ $1'$	1	1
k	2	2 0 -2	0	0

Table 3 Assignments of S_3 representations and weights in Model II

	$(e,\mu)_L$, τ_L	e^c, μ^c, τ^c	H_u	H_d
$SU(2)$	2	1	2	2
S_3	2 $1'$	1 $1'$ $1'$	1	1
k	4	2 0 -2	0	0

4 Γ_2 modular invariant model

4.1 Mass matrices of leptons

In the Γ_2 modular invariant model, the successful lepton mass matrices are presented in Ref. [76]. There are two-type charge lepton mass matrices. The first one is the minimal model I, where the weight 2 and 4 modular forms used, and the second one is the hierarchical model II, where the weight 2 and 6 modular forms appear.

Let us discuss Model I, in which the assignments of the weights for the relevant chiral superfields as in Table 2.

The superpotential terms of the charged lepton masses $w_{E(\mathrm{I})}$ are written as:

$$w_{E(\mathrm{I})} = \alpha_1 e^c H_d[(e,\mu)_L \mathbf{Y}^{(4)}_{\mathbf{2}}]_{\mathbf{1}} + \beta_1 \mu^c H_d[(e,\mu)_L \mathbf{Y}^{(2)}_{\mathbf{2}}]_{\mathbf{1}'} + \gamma_1 \tau^c H_d \tau_L. \tag{35}$$

The charged lepton mass matrix is given as:

$$\mathrm{I}: \quad M_E = v_d \begin{pmatrix} \alpha_1 Y^{(4)}_1 & \alpha_1 Y^{(4)}_2 & 0 \\ \beta_1 Y_2 & -\beta_1 Y_1 & 0 \\ 0 & 0 & \gamma_1 \end{pmatrix}_{RL}, \tag{36}$$

where α_1, β_1 and γ_1 are taken to be real positive parameters without loss of generality, and v_d denotes the VEV of H_d.

It is given approximately by using Eqs. (11) and (13) as:

$$\mathrm{I}: \quad M_E \simeq v_d \begin{pmatrix} -\tilde{\alpha}_1(1-144\epsilon p) & 16\sqrt{3}\tilde{\alpha}_1\sqrt{\epsilon}p' & 0 \\ 8\sqrt{3}\tilde{\beta}_1\sqrt{\epsilon}p' & -\tilde{\beta}_1(1+24\epsilon p) & 0 \\ 0 & 0 & \gamma_1 \end{pmatrix}_{RL}, \tag{37}$$

where

$$\tilde{\alpha}_1 = \left(\frac{7}{100}\right)^2 \alpha_1, \qquad \tilde{\beta}_1 = \left(\frac{7}{100}\right) \beta_1, \tag{38}$$

while γ_1 is remained.

Next, we show Model II, in which the assignments of the weights for the relevant chiral superfields as in Table 3.

The superpotential terms of the charged lepton masses $w_{E(\mathrm{II})}$ are given

$$w_{E(\mathrm{II})} = \alpha_2 e^c H_d[(e,\mu)_L \mathbf{Y}^{(6)}_{\mathbf{2}}]_{\mathbf{1}} + \beta_2 \mu^c H_d[(e,\mu)_L \mathbf{Y}^{(2)}_{\mathbf{2}}]_{\mathbf{1}'} + \gamma_2 \tau^c H_d \tau_L + \alpha_D e^c H_d \tau_L \mathbf{Y}^{(6)}_{\mathbf{1}'}. \tag{39}$$

The charged lepton mass matrix is given in terms of $\mathbf{1}'$ modular form with weigh 6 in addition to S_3 doublet modular forms with weight 2 and 6 as:

$$\mathrm{II}: \quad M_E = v_d \begin{pmatrix} \alpha_2 Y^{(6)}_1 & \alpha_2 Y^{(6)}_2 & \alpha_D \mathbf{Y}^{(6)}_{\mathbf{1}'} \\ \beta_2 Y_2 & -\beta_2 Y_1 & 0 \\ 0 & 0 & \gamma_2 \end{pmatrix}_{RL}, \tag{40}$$

where $\alpha_2, \alpha_D, \beta_2$ and γ_2 are real positive parameters without loss of generality. It is given approximately as:

$$\mathrm{II}: \quad M_E \simeq v_d \begin{pmatrix} \tilde{\alpha}_2(1+264\epsilon p) & 8\sqrt{3}\tilde{\alpha}_2\sqrt{\epsilon}p' & -24\sqrt{3}\tilde{\alpha}_D\sqrt{\epsilon}p' \\ 8\sqrt{3}\tilde{\beta}_2\sqrt{\epsilon}p' & -\tilde{\beta}_2(1+24\epsilon p) & 0 \\ 0 & 0 & \gamma_2 \end{pmatrix}_{RL}, \tag{41}$$

where

$$\tilde{\alpha}_2 = \left(\frac{7}{100}\right)^3 \alpha_2, \quad \tilde{\alpha}_D = \left(\frac{7}{100}\right)^3 \alpha_D, \quad \tilde{\beta}_2 = \left(\frac{7}{100}\right) \beta_2, \tag{42}$$

while γ_2 is remained.

On the other hand, the Weinberg operator gives the neutrino mass matrix, which is common for Model I and Model II:

$$M_\nu = 2g\frac{v_u^2}{\Lambda}\left[\begin{pmatrix} Y_1^2 - Y_2^2 & 2Y_1Y_2 & 2\frac{g'}{2g}Y_1Y_2 \\ 2Y_1Y_2 & Y_2^2 - Y_1^2 & \frac{g'}{2g}(Y_1^2 - Y_2^2) \\ 2\frac{g'}{2g}Y_1Y_2 & \frac{g'}{2g}(Y_1^2 - Y_2^2) & 0 \end{pmatrix} + (Y_1^2 + Y_2^2)\begin{pmatrix} \frac{g''}{g} & 0 & 0 \\ 0 & \frac{g''}{g} & 0 \\ 0 & 0 & \frac{g_p}{g} \end{pmatrix}\right], \tag{43}$$

where the g', g'' and g_p are real positive parameters. It is noted that CP is violated by fixing the modulus τ since the imaginary part of the lepton mass matrices appear through $\mathrm{Re}\,\tau$.

However, we do not discuss details of the neutrino mass matrix in this work because its contribution to our result is negligibly small due to small neutrino masses.

4.2 Wilson coefficients of the leptonic dipole operator

The leptonic dipole operator is written in the flavor space as seen in Eq. (22), where the charged lepton mass matrix is non-diagonal, and given in Eqs. (36) or (40).

In Model I, the flavor structure of $\underset{RL}{\mathcal{C}_{e\gamma}}$ is the same as the Yukawa couplings Y_{RL} apart from coefficients α_1', β_1' and γ_1'. It is given approximately by using Eq. (13) as:

$$\begin{aligned}\text{I}: \ \underset{RL}{\mathcal{C}_{e\gamma}} &= \begin{pmatrix} \underset{ee}{\mathcal{C}_{e\gamma}} & \underset{e\mu}{\mathcal{C}_{e\gamma}} & \underset{e\tau}{\mathcal{C}_{e\gamma}} \\ \underset{\mu e}{\mathcal{C}_{e\gamma}} & \underset{\mu\mu}{\mathcal{C}_{e\gamma}} & \underset{\mu\tau}{\mathcal{C}_{e\gamma}} \\ \underset{\tau e}{\mathcal{C}_{e\gamma}} & \underset{\tau\mu}{\mathcal{C}_{e\gamma}} & \underset{\tau\tau}{\mathcal{C}_{e\gamma}} \end{pmatrix} \\ &\simeq \begin{pmatrix} -\tilde{\alpha}_1'(1-144\epsilon p) & 16\sqrt{3}\tilde{\alpha}_1'\sqrt{\epsilon}p' & 0 \\ 8\sqrt{3}\tilde{\beta}_1'\sqrt{\epsilon}p' & -\tilde{\beta}_1'(1+24\epsilon p) & 0 \\ 0 & 0 & \gamma_1' \end{pmatrix}_{RL}, \end{aligned} \tag{44}$$

where

$$\tilde{\alpha}_1' = \left(\frac{7}{100}\right)^2 \alpha_1', \qquad \tilde{\beta}_1' = \left(\frac{7}{100}\right)\beta_1'. \tag{45}$$

Coefficients α_1', β_1' and γ_1' are different from α_1, β_1 and γ_1 in Eq. (36). Those are complex parameters in contrast to real positive α_1, β_1 and γ_1.

In Model II, it is given approximately as:

$$\begin{aligned}\text{II}: \ \underset{RL}{\mathcal{C}_{e\gamma}} &= \begin{pmatrix} \underset{ee}{\mathcal{C}_{e\gamma}} & \underset{e\mu}{\mathcal{C}_{e\gamma}} & \underset{e\tau}{\mathcal{C}_{e\gamma}} \\ \underset{\mu e}{\mathcal{C}_{e\gamma}} & \underset{\mu\mu}{\mathcal{C}_{e\gamma}} & \underset{\mu\tau}{\mathcal{C}_{e\gamma}} \\ \underset{\tau e}{\mathcal{C}_{e\gamma}} & \underset{\tau\mu}{\mathcal{C}_{e\gamma}} & \underset{\tau\tau}{\mathcal{C}_{e\gamma}} \end{pmatrix} \\ &\simeq \begin{pmatrix} \tilde{\alpha}_2'(1+264\epsilon p) & 8\sqrt{3}\tilde{\alpha}_2'\sqrt{\epsilon}p' & -24\sqrt{3}\tilde{\alpha}_D'\sqrt{\epsilon}p' \\ 8\sqrt{3}\tilde{\beta}_2'\sqrt{\epsilon}p' & -\tilde{\beta}_2'(1+24\epsilon p) & 0 \\ 0 & 0 & \gamma_2' \end{pmatrix}_{RL}, \end{aligned} \tag{46}$$

where

$$\begin{aligned}\tilde{\alpha}_2' &= \left(\frac{7}{100}\right)^3 \alpha_2', \qquad \tilde{\alpha}_D' = \left(\frac{7}{100}\right)^3 \alpha_D', \\ \tilde{\beta}_2' &= \left(\frac{7}{100}\right)\beta_2'. \end{aligned} \tag{47}$$

Coefficients α_2', β_2', α_D' and γ_2' are different from α_2, β_2, α_D and γ_2 in Eq. (40) and complex parameters in general.

The mass matrix M_E in Eqs. (37) and (41) is diagonalized by the bi-unitary transformation $U_R^\dagger M_E U_L$. We can obtain U_L and U_R by diagonalizing $U_L^\dagger M_E^\dagger M_E U_L$ and $U_R^\dagger M_E M_E^\dagger U_R$, respectively. Finally, we obtain $\underset{RL}{\mathcal{C}'_{e\gamma}}$ in the real diagonal basis of the charged lepton mass matrix as $\underset{RL}{\mathcal{C}'_{e\gamma}} = U_R^\dagger \underset{RL}{\mathcal{C}_{e\gamma}} U_L$ for both Model I and Model II. Approximate matrices of U_L and U_R are given in Appendix C and D for Model I and Model II, respectively.

5 Wilson coefficients in mass basis

5.1 Wilson coefficients in Model I

In the flavor basis, the Wilson coefficients are given in Eq. (44) for Model I. We move to the basis of the diagonal mass matrix of the charged leptons as follows:

$$\begin{aligned}\underset{RL}{\mathcal{C}'_{e\gamma}} \simeq U_{R1}^T P_{R1}^* &\begin{pmatrix} -\tilde{\alpha}_1'(1-144\epsilon p) & 16\sqrt{3}\tilde{\alpha}_1'\sqrt{\epsilon}p' & 0 \\ 8\sqrt{3}\tilde{\beta}_1'\sqrt{\epsilon}p' & -\tilde{\beta}_1'(1+24\epsilon p) & 0 \\ 0 & 0 & \gamma_1' \end{pmatrix} \\ &P_{L1}U_{L1}, \end{aligned} \tag{48}$$

where P_{L1}, U_{L1}, P_{R1} and U_{R1}, are given in Eqs. (84), (86), (93) and (94) of Appendix C, respectively. Here, we take $\tilde{\alpha}_1 \ll \tilde{\beta}_1$ and $|\tilde{\alpha}_1'| \ll |\tilde{\beta}_1'|$.

We obtain the Wilson coefficients up to $\mathcal{O}(\sqrt{\epsilon})$ as follows::

$$\begin{aligned}&\underset{ee}{\mathcal{C}'_{e\gamma}} \simeq -\tilde{\alpha}_1', \qquad \underset{\mu\mu}{\mathcal{C}'_{e\gamma}} \simeq -\tilde{\beta}_1', \qquad \underset{\tau\tau}{\mathcal{C}'_{e\gamma}} = \gamma_1', \\ &\underset{e\mu}{\mathcal{C}'_{e\gamma}} \simeq 8\sqrt{3}\tilde{\alpha}_1'\sqrt{\epsilon}e^{-i(\phi_R+\pi\tau_R)} \\ &\left[1 + 2e^{2i\pi\tau_R} - \frac{\tilde{\alpha}_1}{\tilde{\alpha}_1'}\frac{\tilde{\beta}_1'}{\tilde{\beta}_1}e^{i(\phi_R+\pi\tau_R)}\sqrt{5+4\cos 2\pi\tau_R}\right] \\ &\quad = 8\sqrt{3}\tilde{\alpha}_1'\sqrt{\epsilon}\sqrt{5+4\cos 2\pi\tau_R}\left(1 - \frac{\tilde{\alpha}_1}{\tilde{\alpha}_1'}\frac{\tilde{\beta}_1'}{\tilde{\beta}_1}\right), \\ &\underset{\mu e}{\mathcal{C}'_{e\gamma}} \simeq 8\sqrt{3}\tilde{\alpha}_1'\frac{\tilde{\alpha}_1}{\tilde{\beta}_1}\sqrt{\epsilon} \\ &\left[-\frac{\tilde{\alpha}_1}{\tilde{\alpha}_1'}\frac{\tilde{\beta}_1'}{\tilde{\beta}_1}(1+2e^{-2i\pi\tau_R})e^{i(\phi_R+\pi\tau_R)} + \sqrt{5+4\cos 2\pi\tau_R}\right] \\ &\quad = 8\sqrt{3}\tilde{\alpha}_1'\frac{\tilde{\alpha}_1}{\tilde{\beta}_1}\sqrt{\epsilon}\sqrt{5+4\cos 2\pi\tau_R}\left(1 - \frac{\tilde{\alpha}_1}{\tilde{\alpha}_1'}\frac{\tilde{\beta}_1'}{\tilde{\beta}_1}\right), \\ &\underset{e\tau}{\mathcal{C}'_{e\gamma}} = \underset{\tau e}{\mathcal{C}'_{e\gamma}} = 0, \qquad \underset{\mu\tau}{\mathcal{C}'_{e\gamma}} = \underset{\tau\mu}{\mathcal{C}'_{e\gamma}} = 0. \end{aligned} \tag{49}$$

It is noted that $\underset{e\mu}{\mathcal{C}'_{e\gamma}}$ and $\underset{\mu e}{\mathcal{C}'_{e\gamma}}$ vanish if $\tilde{\alpha}_1' = \tilde{\alpha}_1$ and $\tilde{\beta}_1' = \tilde{\beta}_1$ are put. In this model, e-τ and μ-τ transitions never occur. It is also remarked that the imaginary part of Wilson coefficients vanish in full orders of ϵ if $\tilde{\alpha}_1'$, $\tilde{\beta}_1'$ and $\tilde{\gamma}_1'$ are real. That is, the imaginary parts of $\tilde{\alpha}_1'$, $\tilde{\beta}_1'$ and $\tilde{\gamma}_1'$ are the origin of the leptonic EDM.

Taking a constraint of Eq. (32), we have

$$\left|\frac{\mathrm{Im}\,\tilde{\alpha}'_1}{\mathrm{Re}\,\tilde{\beta}'_1}\right| < 1.8\times 10^{-8}. \tag{50}$$

Thus, the imaginary part of α'_1 should be tiny. This tiny imaginary part is discussed in the standpoint of *Stringy Anzatz* in the next section.

5.2 Wilson coefficients in Model II

In the Model II, the Wilson coefficients are given in Eq. (46). In the basis of the diagonal mass matrix of the charged leptons, we have: as follows:

$$\begin{aligned}
&\underset{RL}{\mathcal{C}'_{e\gamma}} \simeq v_d U^T_{R2} P^*_{R2} \\
&\begin{pmatrix} \tilde{\alpha}'_2(1+264\epsilon p) & 8\sqrt{3}\tilde{\alpha}'_2\sqrt{\epsilon}\,p' & -24\sqrt{3}\tilde{\alpha}'_D\sqrt{\epsilon}\,p' \\ 8\sqrt{3}\tilde{\beta}'_2\sqrt{\epsilon}\,p' & -\tilde{\beta}'_2(1+24\epsilon p) & 0 \\ 0 & 0 & \gamma'_2 \end{pmatrix} \\
&P_{L2}U_{L2},
\end{aligned} \tag{51}$$

where P_{L2}, U_{L2}, P_{R2} and U_{R2}, are given in Eqs. (107), (109), (116) and (118) of Appendix D, respectively. Here, we take $\tilde{\alpha}_2 \sim \tilde{\alpha}_D \ll \tilde{\beta}_2 \ll \gamma_2$ and $|\tilde{\alpha}'_2| \sim |\tilde{\alpha}'_D| \ll |\tilde{\beta}'_2| \ll |\tilde{\gamma}'_2|$.

The Wilson coefficients are given explicitly up to $\mathcal{O}(\sqrt{\epsilon})$ as follows:

$$\begin{aligned}
&\underset{ee}{\mathcal{C}'_{e\gamma}} \simeq \tilde{\alpha}'_2, \quad \underset{\mu\mu}{\mathcal{C}'_{e\gamma}} \simeq -\tilde{\beta}'_2, \quad \underset{\tau\tau}{\mathcal{C}'_{e\gamma}} \simeq \gamma'_2, \\
&\underset{e\mu}{\mathcal{C}'_{e\gamma}} \simeq 8\sqrt{3}\tilde{\alpha}'_2\sqrt{\epsilon}\, i e^{-i\pi\tau_R} \\
&\quad \left(-1 + e^{2i\pi\tau_R} - 2i\,\frac{\alpha_2}{\alpha'_2}\frac{\beta'_2}{\beta_2} e^{i\pi\tau_R}\sin\pi\tau_R\right) \\
&\quad = -16\sqrt{3}\tilde{\alpha}'_2\sqrt{\epsilon}\,\sin\pi\tau_R\left(1 - \frac{\alpha_2}{\alpha'_2}\frac{\beta'_2}{\beta_2}\right), \\
&\underset{\mu e}{\mathcal{C}'_{e\gamma}} \simeq 8\, i\, e^{i\pi\tau_R}\sqrt{3}\tilde{\beta}'_2\frac{\tilde{\alpha}^2_2}{\tilde{\beta}^2_2}\sqrt{\epsilon} \\
&\quad \left(-1 + e^{-2i\pi\tau_R} + 2i\,\frac{\alpha'_2}{\alpha_2}\frac{\beta_2}{\beta'_2} e^{-i\pi\tau_R}\sin\pi\tau_R\right) \\
&\quad = 16\sqrt{3}\tilde{\beta}'_2\frac{\tilde{\alpha}^2_2}{\tilde{\beta}^2_2}\sin\pi\tau_R\sqrt{\epsilon}\left(1 - \frac{\alpha'_2}{\alpha_2}\frac{\beta_2}{\beta'_2}\right), \\
&\underset{e\tau}{\mathcal{C}'_{e\gamma}} \simeq -24\sqrt{3}\tilde{\alpha}'_D\sqrt{\epsilon}\left(1 - \frac{\tilde{\alpha}_D}{\tilde{\alpha}'_D}\frac{\gamma'_2}{\gamma_2}\right), \\
&\underset{\tau e}{\mathcal{C}'_{e\gamma}} \simeq -24\sqrt{3}\alpha'_2\frac{\tilde{\alpha}_D}{\gamma_2}\sqrt{\epsilon}\left(1 - \frac{\tilde{\alpha}_2}{\tilde{\alpha}'_2}\frac{\gamma'_2}{\gamma_2}\right), \\
&\underset{\mu\tau}{\mathcal{C}'_{e\gamma}} \sim \tilde{\alpha}'_D\,\mathcal{O}\left(\frac{\tilde{\alpha}_2}{\tilde{\beta}_2}\epsilon\right), \quad \underset{\tau\mu}{\mathcal{C}'_{e\gamma}} \sim \tilde{\alpha}'_2\,\mathcal{O}\left(\frac{\tilde{\alpha}_D}{\gamma_2}\epsilon\right).
\end{aligned} \tag{52}$$

It is easily found that $\underset{e\mu}{\mathcal{C}'_{e\gamma}}$ and $\underset{\mu e}{\mathcal{C}'_{e\gamma}}$ vanish if $\tilde{\alpha}'_2 = \tilde{\alpha}_2$ and $\tilde{\beta}'_2 = \tilde{\beta}_2$ are put. The coefficient $\underset{e\tau}{\mathcal{C}'_{e\gamma}}$ ($\underset{\tau e}{\mathcal{C}'_{e\gamma}}$) also vanishes if $\tilde{\alpha}'_D = \tilde{\alpha}_D$ ($\tilde{\alpha}'_2 = \tilde{\alpha}_2$) and $\tilde{\gamma}'_2 = \tilde{\gamma}_2$ are impose. Since other coefficients $\underset{\tau e}{\mathcal{C}'_{e\gamma}}, \underset{\mu\tau}{\mathcal{C}'_{e\gamma}}$ and $\underset{\tau\mu}{\mathcal{C}'_{e\gamma}}$ are suppressed, we present them in order estimates.

It is also remarked that the imaginary part of Wilson coefficients vanish in full orders of ϵ if $\tilde{\alpha}'_2$, $\tilde{\beta}'_2$ and $\tilde{\gamma}'_2$ are real. That is, the imaginary part of $\tilde{\alpha}'_2$, $\tilde{\beta}'_2$ and $\tilde{\gamma}'_2$ lead to the leptonic EDM.

Taking a constraint of Eq. (32), the imaginary part of α'_2 should be also tiny as discussed in Sect. 5.1.

6 Numerical analyses

6.1 Parametrization

As discussed in Sect. 3.2, the lightest mode "m" corresponds to Higgs doublet H in *Stringy Ansatz* of Eq. (1). If the mode "m" is only H, the flavor structure of bilinear operator $[\,\bar{E}_R\sigma^{\mu\nu}E_L\,]$ is exactly the same as the mass matrix. Therefore, the LFV process such as $\mu \to e$ never happen.

However, additional unknown modes "m" in Eq. (1) cause the flavor violation. We discuss such a case in our numerical analysis. Let us introduce a small parameter δ_α to see the difference between $\tilde{\alpha}_{1(2)}$ and $\tilde{\alpha}'_{1(2)}$. In the same way, δ_β, δ_γ and δ_D are introduced. They are expected to be of the same order and given as follows:

$$\begin{aligned}
&\frac{\tilde{\alpha}'_{1(2)}}{\tilde{\alpha}_{1(2)}} = 1+\delta_\alpha, \quad \frac{\tilde{\beta}'_{1(2)}}{\tilde{\beta}_{1(2)}} = 1+\delta_\beta, \\
&\frac{\tilde{\gamma}'_{1(2)}}{\tilde{\gamma}_{1(2)}} = 1+\delta_\gamma, \quad \frac{\tilde{\alpha}'_D}{\tilde{\alpha}_D} = 1+\delta_D,
\end{aligned} \tag{53}$$

where $\delta_\alpha, \delta_\beta, \delta_\gamma$ and δ_D are complex and tiny from unknown modes of "m" in Eq. (1), which may be higher excited modes of Higgs.

Indeed, if δ_α, δ_β, δ_γ and δ_D vanish, off diagonal Wilson coefficients vanishes as seen in Eqs. (49) and (52) of Sect. 5 up to $\mathcal{O}(\sqrt{\epsilon})$. We constrain those small parameters by inputting the experimental upper-bounds in Sect. 3.1.

In the following analyses, small parameters δ_α et al. are put statistically in the normal distribution with an average 0 and standard deviation σ. Then, we can take $|\delta_\alpha| \simeq |\delta_\beta| \simeq |\delta_\gamma| \simeq |\delta_D| \simeq \sigma$ as seen in Appendix E.

6.2 Input parameter

Since we adopt the Γ_2 modular flavor models in Ref. [76], the parameters of charged lepton mass matrix are fixed. We list them for the charged lepton sector in Table 4 as follows:

Table 4 Best fit values of parameters of the charged leptons in Γ_2 modular flavor model [76], where α, β and γ correspond to α_1, β_1 and γ_1 for Model I, and α_2, β_2 and γ_2 for Model II, respectively. Values in "Seesaw Model" are also listed [77]

	Model I	Model II	"Seesaw Model"
τ	$\pm 0.0895 + 1.697\,i$	$\pm 0.090 + 1.688\,i$	$\pm 0.244 + 1.132\,i$
β/α	14.33	1.03	0.92
γ/α	17.39	1.26	-1.20
α_D/α	–	1.33	$10^{-13.4}$

We have not discussed the "Seesaw Model" in Table 4 since the charged lepton mass matrix is the same flavor structure as Model II. We only comment on the numerical result for "Seesaw Model" in Summary of section 7. We use these values in our numerical calculations.

6.3 Constraints of δ_α and δ_β from $|d_e|$ and $\mathcal{B}(\mu \to e\gamma)$

The tight constraints come from the experimental upper-bounds of $|d_e|$ and $\mathcal{B}(\mu \to e\gamma)$. The relevant Wilson coefficients $\underset{ee}{\mathcal{C}'_{e\gamma}}$ and $\underset{e\mu}{\mathcal{C}'_{e\gamma}}$ are given in Eqs. (49) and (52). Let us consider the Model I to see the magnitude of constraint from $|d_e|$ and $\mathcal{B}(\mu \to e\gamma)$. By using the approximate forms in Eq. (127) of Appendix E, we have a simple expressions of the ratio of the Wilson coefficients:

$$\left|\frac{\underset{e\mu}{\mathcal{C}'_{e\gamma}}}{\underset{\mu\mu}{\mathcal{C}'_{e\gamma}}}\right| \simeq 8\sqrt{3}\sqrt{\epsilon}\sqrt{5+4\cos 2\pi\tau_R}\left|\frac{\tilde{\alpha}'_1}{\tilde{\beta}'_1}\left(1-\frac{\tilde{\alpha}_1}{\tilde{\alpha}'_1}\frac{\tilde{\beta}'_1}{\tilde{\beta}_1}\right)\right|$$
$$\simeq 8\sqrt{3}\sqrt{\epsilon}\sqrt{5+4\cos 2\pi\tau_R}\left|\frac{\tilde{\alpha}'_1}{\tilde{\beta}'_1}\right|\sigma. \tag{54}$$

Putting the numerical values of Model I in Table 4, we have

$$\left|\frac{\underset{e\mu(\mu e)}{\mathcal{C}'_{e\gamma}}}{\underset{\mu\mu}{\mathcal{C}'_{e\gamma}}}\right| \simeq 10^{-3}\sigma, \tag{55}$$

where $|\tilde{\alpha}'_1/\tilde{\beta}'_1| \simeq (7/100)\times\alpha_1/\beta_1$ and $\sqrt{\epsilon} = 5\times 10^{-3}$ are used. Since the upper-bound of this ratio is 1.8×10^{-5} as seen in Eq. (26), we have

$$\sigma \simeq |\delta_\alpha| \simeq |\delta_\beta| < 10^{-2}. \tag{56}$$

Indeed, in our numerical calculations, the statistical parameters δ_α and δ_β with the average 0 and $\sigma = 0.01$ reproduce $\mathcal{B}(\mu \to e\gamma)$ consistent with the experimental upper-bound.

It is remarked that the NP signal of the $\mu \to e\gamma$ process comes from the operator $\bar{e}_R\sigma_{\mu\nu}\mu_L$ mainly in our scheme because we have a ratio

$$\left|\frac{\underset{\mu e}{\mathcal{C}'_{e\gamma}}}{\underset{e\mu}{\mathcal{C}'_{e\gamma}}}\right| \simeq \left|\frac{\tilde{\alpha}_1}{\tilde{\beta}_1}\right| = \frac{7}{100}\frac{\alpha_1}{\beta_1} \simeq 5\times 10^{-3}, \tag{57}$$

from Eq. (49) and Table 4. This prediction is contrast to the prediction of the $\bar{\mu}_R\sigma_{\mu\nu}e_L$ dominant decay in the $U(2)$ flavor model [38]. The angular distribution with respect to the muon polarization can distinguish between $\mu^+ \to e^+_L\gamma$ and $\mu^+ \to e^+_R\gamma$ [105].

On the other hand, the constraint of $|d_e|$ is very tight. As seen in Eq. (49),

$$\frac{\mathrm{Im}\,[\underset{e\mu(\mu e)}{\mathcal{C}'_{e\gamma}}]}{\mathrm{Re}\,[\underset{\mu\mu}{\mathcal{C}'_{e\gamma}}]} \simeq \left|\frac{\tilde{\alpha}_1}{\tilde{\beta}_1}\right|\mathrm{Im}\,\delta_\alpha. \tag{58}$$

Since the upper-bound of this ratio is 10^{-8} as seen in Eq. (32), we have

$$\mathrm{Im}\,\delta_\alpha < 10^{-6}. \tag{59}$$

The constraints of Eqs. (56) and (59) suggest us that the electron EDM gives stronger constraint than the $\mu \to e\gamma$ decay for NP if the phase of δ_α is of order one. Then, the $\mu \to e\gamma$ decay is much suppressed compared with the present experimental upper-bound. This numerical prediction is presented in the next subsection. However, if δ_α is real, the electron EDM does not give constraint for NP, but its magnitude is a prediction through the next-to-leading contribution, which is omitted in Eq. (49). The numerical results are also presented in this case in the next subsections.

6.4 Electron $(g-2)_e$

The NP of $(g-2)_\mu$ and $(g-2)_e$ appears in the diagonal components of the Wilson coefficient of the dipole operator at the mass basis. We have the ratios of the diagonal coefficients from Eq. (49) as:

$$\frac{\mathrm{Re}\,\underset{ee}{\mathcal{C}'_{e\gamma}}}{\mathrm{Re}\,\underset{\mu\mu}{\mathcal{C}'_{e\gamma}}} \simeq \left|\frac{\tilde{\alpha}_{1(2)}}{\tilde{\beta}_{1(2)}}\right| \simeq 4.9\,(4.8)\times 10^{-3}, \tag{60}$$

where numerical values of Table 4 are put for $\beta_{1(2)}/\alpha_{1(2)}$. These predicted ratios are almost in agreement with the charged lepton mass ratio $m_e/m_\mu = 4.84 \times 10^{-3}$.

By inputting the experimental value of Eq. (14), the real part of the Wilson coefficient of the muon $\mathcal{C}'_{\substack{e\gamma \\ \mu\mu}}$ has been obtained as seen in Eq. (24) [37]. Now, we can estimate the magnitude of the electron $(g-2)_e$ anomaly by using the relation in Eq. (60) as:

$$\Delta a_e = \frac{4m_e}{e}\frac{v}{\sqrt{2}}\frac{1}{\Lambda^2}\mathrm{Re}\,[\mathcal{C}'_{\substack{e\gamma \\ ee}}] \simeq 5.8 \times 10^{-14}. \tag{61}$$

It is easily seen that Δa_e and Δa_μ are proportional to the lepton masses squared. This result is in agreement with the naive scaling $\Delta a_\ell \propto m_\ell^2$ [106].

In the electron anomalous magnetic moment, the experiments [107] give

$$a_e^{\mathrm{Exp}} = 1\,159\,652\,180.73(28) \times 10^{-12}, \tag{62}$$

while the SM prediction crucially depends on the input value for the fine-structure constant α. Two latest determination [108,109] based on Cesium and Rubidium atomic recoils differ by more than 5σ. Those observations lead to the difference from the SM prediction:

$$\begin{aligned}\Delta a_e^{Cs} &= a_e^{\mathrm{Exp}} - a_e^{\mathrm{SM,CS}} = (-8.8 \pm 3.6) \times 10^{-13},\\ \Delta a_e^{Rb} &= a_e^{\mathrm{Exp}} - a_e^{\mathrm{SM,Rb}} = (4.8 \pm 3.0) \times 10^{-13}.\end{aligned} \tag{63}$$

Our predicted value is smaller of order one than the observed one at present. We need the precise observation of the fine structure constant to test our model.

6.5 Electron EDM and $\mu \to e\gamma$ decay

The LFV process is severely constrained by the experimental bound $\mathcal{B}(\mu^+ \to e^+\gamma) < 3.1 \times 10^{-13}$ by the combination of the MEG and MEG II experiments [26,27]. As seen in Sect. 6.3, the parameter δ_α and δ_β are constrained in Eq. (56). On the other hand, the constraint of $|d_e|$ by the JILA experiment [18] is much tight compared with the one from $\mathcal{B}(\mu^+ \to e^+\gamma)$ as seen in Eq. (59).

At first, suppose the phase of δ_α being of order one. Then, the upper-bound of the absolute value of δ_α is around 10^{-6} as seen in Eq. (59). Since δ_β and δ_γ are also of the same order 10^{-6} (See Eq. (53)), we can estimate the branching ratio of the $\mu \to e\gamma$ decay by taking $\sigma \simeq |\delta_\alpha| \simeq |\delta_\beta| \simeq |\delta_\gamma|$ as presented in Appendix E.

In Fig. 1, we plot $\mathcal{B}(\mu \to e\gamma)$ versus the electron EDM $|d_e|$ taking $\sigma = 10^{-6}$ in Model I. It is found that the electron EDM is almost consistent with the experimental upper-bound. Then, the branching ratio of the $\mu \to e\gamma$ decay is at

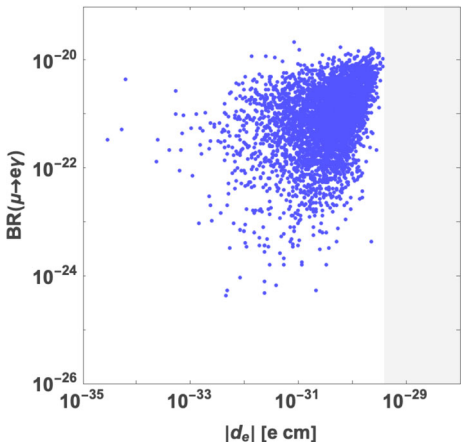

Fig. 1 Plot of $\mathcal{B}(\mu \to e\gamma)$ versus $|d_e|$ in Model I, where $\sigma = 10^{-6}$ is put. The grey region is excluded by the experimental upper-bound of $|d_e|$

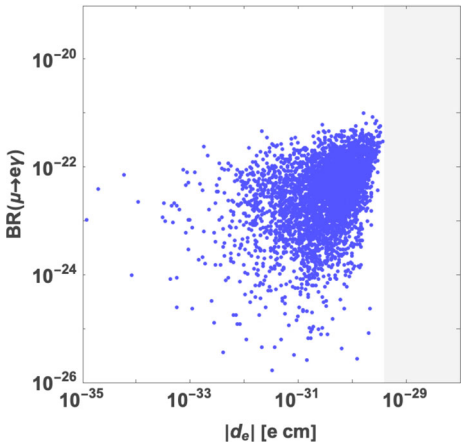

Fig. 2 Plot of $\mathcal{B}(\mu \to e\gamma)$ versus $|d_e|$ in Model II, where $\sigma = 10^{-6}$ is put. The grey region is excluded by the experimental upper-bound of $|d_e|$

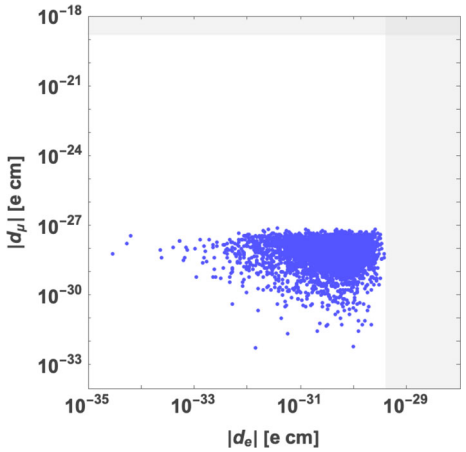

Fig. 3 Plot of $|d_\mu|$ versus $|d_e|$ in Model I where $\sigma = 10^{-6}$ is put. The grey regions are excluded by the experimental upper-bounds of $|d_e|$ and $|d_\mu|$

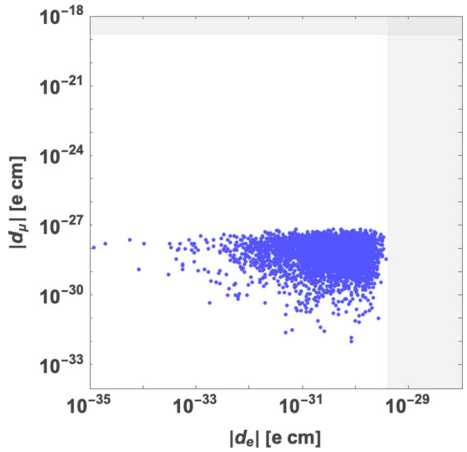

Fig. 4 Plot of $|d_\mu|$ versus $|d_e|$ in Model II, where $\sigma = 10^{-6}$ is put. The grey regions are excluded by the experimental upper-bounds of $|d_e|$ and $|d_\mu|$

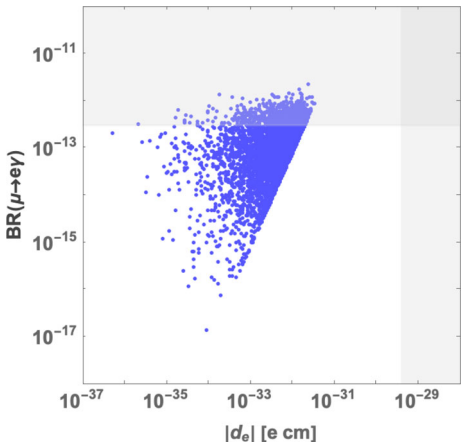

Fig. 5 Branching ratios of $\mu \to e\gamma$ versus $|d_e|$ in Model I with $\sigma = 10^{-2}$ and $\mathrm{Im}\,\delta_\alpha = 0$. The grey regions are excluded by the experimental upper-bounds

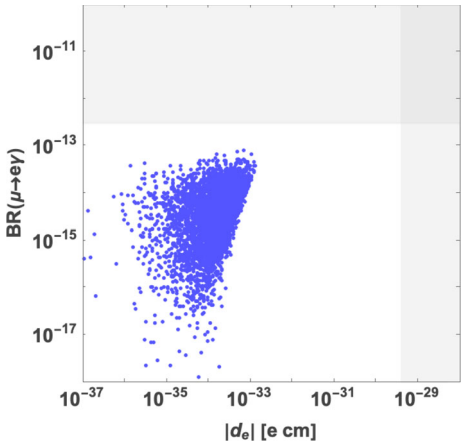

Fig. 6 Branching ratios of $\mu \to e\gamma$ versus $|d_e|$ in Model II with $\sigma = 10^{-2}$ and $\mathrm{Im}\,\delta_\alpha = 0$. The grey regions are excluded by the experimental upper-bounds

most 10^{-20}. In Fig. 2, we also plot $\mathcal{B}(\mu \to e\gamma)$ versus the electron EDM $|d_e|$ taking $\sigma = 10^{-6}$ in Model II. It is found that the branching ratio of the $\mu \to e\gamma$ decay is also at most 10^{-21}. There is no hope to observe the $\mu \to e\gamma$ decay in the near future for both models.

In Fig. 3, we show the muon EDM $|d_\mu|$ versus the electron EDM $|d_e|$ in Model I. The predicted upper-bound of $|d_\mu|$ is around 10^{-27}e cm. In Fig. 4, we also show the muon EDM $|d_\mu|$ versus the electron EDM $|d_e|$ in Model II. The predicted upper-bound of $|d_\mu|$ is also around 10^{-27}e cm. In both models, the ratio of $|d_e/d_\mu|$ is expected to be the mass ratio m_e/m_μ approximately.

Our prediction of $\mathcal{B}(\mu \to e\gamma)$ depends on the value of $\sigma \simeq |\delta_\alpha| \simeq |\delta_\beta|$. The absolute value of δ_α should be lower than around 10^{-2} from the upper-bound of $\mathcal{B}(\mu \to e\gamma)$ as seen in Eq. (56). While $\mathrm{Im}\,\delta_\alpha$ should be much smaller than $|\delta_\alpha|$ to avoid the constraint of electron EDM. If $\mathcal{B}(\mu \to e\gamma)$ will be observed at the little bit below the present experimental upper-bound $\mathcal{O}(10^{-13})$ in the near future, the phase of δ_α is severely suppressed. The simplest expectation is δ_α being real

without fine-tuning of the CP phase. Leptonic EDMs vanish in both Model I and Model II under the condition of real $\delta_\alpha, \delta_\beta$ and δ_γ. It is remarked that the CP phase of the modular form (comes from modulus τ) do not contribute to the EDM as far as $\delta_\alpha, \delta_\beta$ and δ_γ are real because the 3×3 Wilson coefficient matrix has the same phase structure as the charged lepton mass matrix.

However, we can consider the alternative case that δ_β and δ_γ are complex while only δ_α is real. Then, the imaginary part of δ_β can contribute to the electron EDM in the next-to-leading order of ϵ. Indeed, we find

$$|d_e| \sim \frac{\tilde{\alpha}_{1(2)}}{\tilde{\beta}_{1(2)}} \epsilon\, \mathrm{Im}\,\tilde{\beta}'_{1(2)} = \tilde{\alpha}_{1(2)}\, \epsilon\, \mathrm{Im}\,\delta_\beta,$$

$$|d_\mu| \sim \mathrm{Im}\,\tilde{\beta}'_{1(2)} = \tilde{\beta}_{1(2)} \mathrm{Im}\,\delta_\beta, \quad |d_\tau| \sim \mathrm{Im}\,\gamma'_{1(2)} = \gamma_{1(2)} \mathrm{Im}\,\delta_\gamma, \tag{64}$$

where $\mathrm{Im}\,\delta_\beta \sim |\delta_\beta|$ and $\mathrm{Im}\,\delta_\gamma \sim |\delta_\gamma|$. Under this set up of those phases, we predict the leptonic EDM in Model I and Model II.

In Fig. 5, we show $\mathcal{B}(\mu \to e\gamma)$ versus $|d_e|$ taking $\sigma = 10^{-2}$ with real δ_α in Model I. It is found that the electron EDM is almost below 10^{-32}e cm, which is of two order smaller than the present experimental upper bound, while $\mathcal{B}(\mu \to e\gamma)$ is close to the experimental present upper-bound. In Fig. 6, we also plot $\mathcal{B}(\mu \to e\gamma)$ versus $|d_e|$ taking $\sigma = 10^{-2}$ with real δ_α in Model II. It is found that the branching ration of the $\mu \to e\gamma$ and the electron EDM are smaller than of one order than the ones in Model I.

In Fig. 7, we show also the muon EDM, d_μ versus $|d_e|$ in Model I. The predicted upper-bound of $|d_\mu|$ is rather large

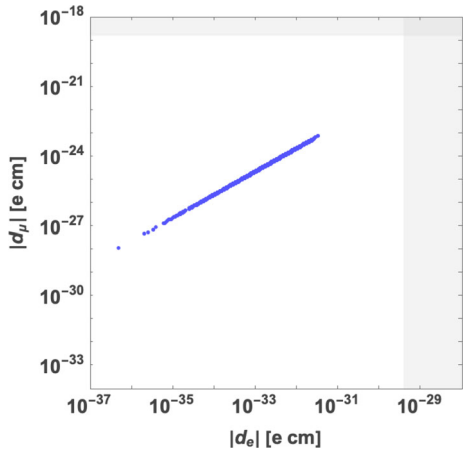

Fig. 7 The muon EDM versus electron EDM in Model I with $\sigma = 10^{-2}$ and Im $\delta_\alpha = 0$. The grey regions are excluded by the experimental upper-bounds

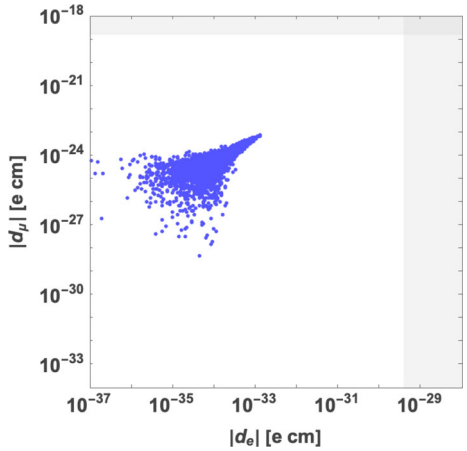

Fig. 8 The muon EDM versus electron EDM in Model II with $\sigma = 10^{-2}$ and Im $\delta_\alpha = 0$. The grey regions are excluded by the experimental upper-bounds

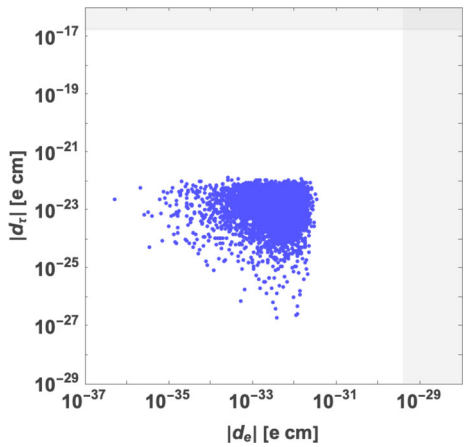

Fig. 9 The tauon EDM versus electron EDM in Model I with $\sigma = 10^{-2}$ and Im $\delta_\alpha = 0$. The grey regions are excluded by the experimental upper-bounds

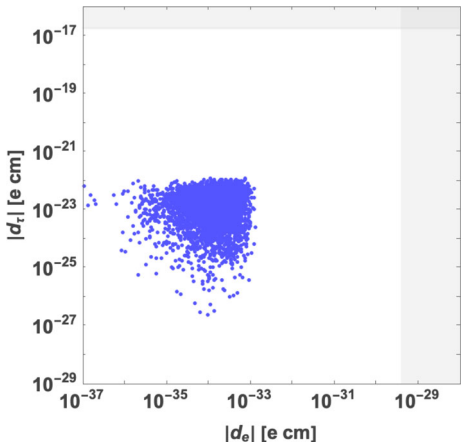

Fig. 10 The tauon EDM versus electron EDM in Model II with $\sigma = 10^{-2}$ and Im $\delta_\alpha = 0$. The grey regions are excluded by the experimental upper-bounds

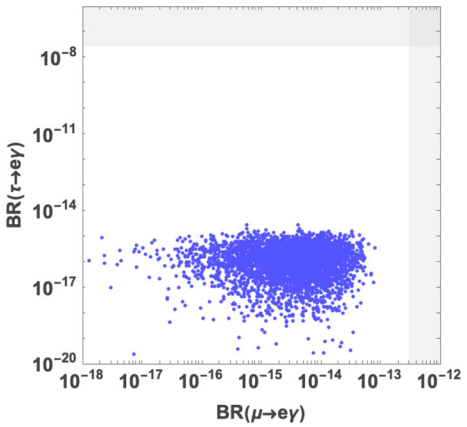

Fig. 11 Branching ratios of $\tau \to e\gamma$ versus $\mu \to e\gamma$ in Model II with $\sigma = 10^{-2}$ and Im $\delta_\alpha = 0$. The grey regions are excluded by the experimental upper-bounds

around 10^{-23} e cm. The both EDMs are almost proportional to each other, which is expected in Eq. (64). In Fig. 8, we show the muon EDM d_μ versus $|d_e|$ in Model II. The predicted upper-bound of $|d_\mu|$ is also around 10^{-23} e cm.

The tauon EDM d_τ is also predicted versus $|d_e|$ for Model I and Model II in Figs. 9 and 10, respectively. The rather large tauon EDM is predicted to be $|d_\tau| \simeq 10^{-22}$ e cm compared with the muon EDM because the ratio of $|d_\mu/d_\tau|$ is expected to be the mass ratio m_μ/m_τ approximately.

6.6 LFV decays of tauon in Model II

In Model I, $\tau \to e\gamma$ and $\tau \to \mu\gamma$ decays never occur because the tauon decouples to the muon and electron as seen in Eq. (37). On the other hand, in Model II , the tauon couples directly the electron as seen in Eq. (41). Therefore, it also couples to the muon in the next-to-leading order. Indeed, we can predict the $\tau \to e\gamma$ and $\tau \to \mu\gamma$ decays numerically.

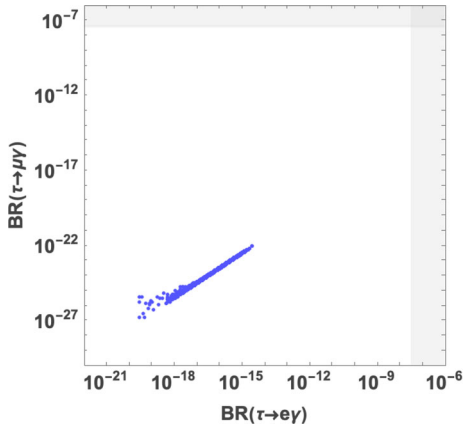

Fig. 12 Branching ratios of $\tau \to e\gamma$ and $\tau \to \mu\gamma$ in Model II with $\sigma = 10^{-2}$ and $\mathrm{Im}\,\delta_\alpha = 0$. The grey regions are excluded by the experimental upper-bounds

Let us take $\sigma = 10^{-2}$, where $\sigma \simeq |\delta_\alpha| \simeq |\delta_\beta| \simeq |\delta_\gamma|$ with $\mathrm{Im}\,\delta_\alpha = 0$. In Fig. 11, we plot the branching ratios of $\tau \to e\gamma$ versus $\mu \to e\gamma$ in Model II. The branching ratios of $\tau \to e\gamma$ is expected to be 10^{-15}.

In Fig. 12, we plot the branching ratios of $\tau \to e\gamma$ and $\tau \to \mu\gamma$.

with $\sigma = 10^{-2}$ and $\mathrm{Im}\,\delta_\alpha = 0$. The branching ratio of $\tau \to \mu\gamma$ is almost proportional to the one of $\tau \to e\gamma$. This behavior is understandable that the $\tau - \mu$ coupling is induced through $\tau - e$ coupling in Model II. The branching ratio is at most 10^{-22}, which is far from the present experimental upper-bound.

7 Summary

We have studied the leptonic EDM and the LFV decays relating with the recent data of anomalous magnetic moment $(g-2)_\mu$ in the leptonic dipole operator. In order to control the 4-point couplings of SMEFT, we employ the relation Eq. (1) as *Stringy Ansatz*, that is, higher-dimensional operators are related with 3-point couplings. We have adopted the Γ_2 modular invariant model to control the flavor structure of leptons, which gives the successful lepton mass matrices [76]. There are two-type mass matrices for the charged leptons. The first one is the minimal model, where the tauon decouples to the muon and the electron. In the second one, the tauon directly couples to the electron.

Suppose the anomaly of the anomalous magnetic moment of the muon Δa_μ to be evidence of NP, we have related it with the anomalous magnetic moment of the electron Δa_e, the electron EDM d_e and the $\mu \to e\gamma$ decay. It is found that the NP contribution to a_e and a_μ is proportional to the lepton masses squared likewise the naive scaling $\Delta a_\ell \propto m_\ell^2$. The predicted value of the anomaly of $(g-2)_e$ is small of one order compared with the observed one at present.

It is also remarked that the NP signal of the $\mu \to e\gamma$ process comes from the operator $\bar{e}_R \sigma_{\mu\nu} \mu_L$ in our scheme. This prediction is contrast to the one in the $U(2)$ flavor model [38].

The constraint of $|d_e|$ by the JILA experiment [18] is much tight compared with the one from $\mathcal{B}(\mu^+ \to e^+\gamma)$ in our framework. Supposing the phase of δ_α being of order one, the upper-bound of the absolute value of δ_α is around 10^{-6}. Since δ_β and δ_γ are also of the same order 10^{-6}, we can estimate the branching ratio of the $\mu \to e\gamma$ decay. Then, the branching ration of the $\mu \to e\gamma$ decay is at most 10^{-20} (10^{-21}) in Model I (II).

The smallness of $|d_e|$ comes from the tiny $\mathrm{Im}\,\delta_\alpha$. If δ_α, δ_β and δ_γ are real, leptonic EDMs vanish in both models since the CP phase of the modular form due to modulus τ do not contribute to EDMs. However, there is a possibility to obtain $\mathcal{B}(\mu \to e\gamma) \simeq 10^{-13}$ while non-vanishing electron EDM. We have considered the case that δ_β and δ_γ are complex while only δ_α is real with $|\delta_\alpha| \simeq |\delta_\beta| \simeq |\delta_\gamma| \simeq 0.01$. Then, the imaginary part of δ_β can contribute to the electron EDM in the next-to-leading order of ϵ. The predicted electron EDM is below 10^{-32} e cm, while $\mathcal{B}(\mu \to e\gamma)$ is close to the experimental present upper-bound in Model I. In Model II, the branching ration of the $\mu \to e\gamma$ and the magnitude of the electron EDM are smaller than of one order than the ones in Model I. The predicted upper-bound of $|d_\mu|$ is rather large, around 10^{-23} e cm and of $|d_\tau|$ is 10^{-22} e cm in both models.

Our prediction of the electron EDM is compared with other ones of models with the non-Abelian flavor symmetry. In the Γ_3 (A_4) modular invariant model, the constraint of $|d_e|$ is much looser than our result. Indeed, $\mathcal{B}(\mu \to e\gamma)$ is bounded lower than $\mathcal{O}(10^{-16})$ by imposing the experimental constraint of $|d_e|$ [63], while it is bounded lower than $\mathcal{O}(10^{-20})$ in our model. On the other hand, $|d_e|$ is predicted near the present upper-bound, $\mathcal{O}(10^{-30} - 10^{-31})$ e cm in the $U(2)_L \otimes U(2)_R$ flavor symmetry [38]. Thus, the prediction of $|d_e|$ depends on the flavor symmetry.

In other words, the observation of the electron EDM is good test to distinguish models with flavor symmetry.

In Model I, $\tau \to e\gamma$ and $\tau \to \mu\gamma$ decays never occur because the tauon decouples to the muon and electron as seen in Eq. (37). On the other hand, in Model II, the tauon couples directly the electron as seen in Eq. (41). Therefore, it also couples to the muon in the next-to-leading order. Taking $\sigma = 10^{-2}$ in Model II , the branching ratios of $\tau \to e\gamma$ is expected to be 10^{-15} and of $\tau \to \mu\gamma$ is at most 10^{-22}, which are far from the present experimental upper-bound.

In our numerical analyses, we do not include the renormalization group (RG) contribution. The RG evolution contribution of the leptonic dipole operators has been discussed in Ref. [37,63] to estimate the RG effect on the numeri-

cal results at the low-energy. Our numerical result is not so changed even if the RG effect is included as well as in Ref. [63].

Finally, it is noted that alternative lepton flavor model with the Γ_2 modular symmetry [77], which is "Seesaw Model" in Table 4 leads to the similar result to the one of Model I. Thus, the modular flavor symmetry is powerful to investigate NP of leptons in the framework of SMEFT if the symmetry is specified.

Acknowledgements The work was supported by the Fundamental Research Funds for the Central Universities (T. N.).

Data Availability Statement This manuscript has no associated data. [Authors' comment: We do not have data for the paper.]

Code Availability Statement This manuscript has no associated code/software. [Authors' comment: We did not use any code in this work.]

Funded by SCOAP[3].

Appendix

A Tensor product of S_3 group

We take the generators of S_3 group for the doublet as follows:

$$S = \frac{1}{2}\begin{pmatrix} -1 & -\sqrt{3} \\ -\sqrt{3} & 1 \end{pmatrix}, \qquad T = \begin{pmatrix} 1 & 0 \\ 0 & -1 \end{pmatrix}. \tag{65}$$

In this basis, the multiplication rules are:

$$\begin{aligned} &\begin{pmatrix} a_1 \\ a_2 \end{pmatrix}_{\mathbf{2}} \otimes \begin{pmatrix} b_1 \\ b_2 \end{pmatrix}_{\mathbf{2}} \\ &= (a_1 b_1 + a_2 b_2)_{\mathbf{1}} \oplus (a_1 b_2 - a_2 b_1)_{\mathbf{1}'} \oplus \frac{1}{3} \\ &\quad \begin{pmatrix} -a_1 b_1 + a_2 b_2 \\ a_1 b_2 + a_2 b_1 \end{pmatrix}_{\mathbf{2}}, \end{aligned} \tag{66}$$

$$\mathbf{1} \otimes \mathbf{1} = \mathbf{1}, \qquad \mathbf{1}' \otimes \mathbf{1}' = \mathbf{1},$$

$$\mathbf{1}' \otimes \begin{pmatrix} a_1 \\ a_2 \end{pmatrix}_{\mathbf{2}} = \begin{pmatrix} -a_2 \\ a_1 \end{pmatrix}_{\mathbf{2}}, \tag{67}$$

where

$$S(\mathbf{1}) = 1, \qquad S(\mathbf{1}') = 1, \qquad T(\mathbf{1}') = 1, \qquad T(\mathbf{1}') = -1. \tag{68}$$

Further details can be found in the reviews [79–81].

B Experimental constraints on the dipole operators

From the experimental data of the muon $(g-2)_\mu$ and $\mu \to e\gamma$, Ref. [37] gave the constraints on the dipole operators. We summarize briefly them on the dipole operators in Eq. (22). Below the scale of electroweak symmetry breaking, the leptonic dipole operators are given as:

$$\mathcal{O}_{\substack{e\gamma \\ rs}} = \frac{v}{\sqrt{2}} \bar{e}_{R_r} \sigma^{\mu\nu} e_{L_s} F_{\mu\nu}, \tag{69}$$

where $\{r, s\}$ are flavor indices e, μ, τ and $F_{\mu\nu}$ is the electromagnetic field strength tensor. The effective Lagrangian is

$$\mathcal{L}_{\text{dipole}} = \frac{1}{\Lambda^2}\left(\mathcal{C}'_{\substack{e\gamma \\ rs}} \mathcal{O}_{\substack{e\gamma \\ rs}} + \mathcal{C}'_{\substack{e\gamma \\ rs}} \mathcal{O}_{\substack{e\gamma \\ rs}}\right), \tag{70}$$

where Λ is a certain mass scale of NP in the effective theory. The corresponding Wilson coefficient $\mathcal{C}'_{\substack{e\gamma \\ rs}}$ is denoted in the mass-eigenstate basis of leptons.

The tree-level expression for Δa_μ in terms of the Wilson coefficient of the dipole operator is

$$\Delta a_\mu = \frac{4 m_\mu}{e} \frac{v}{\sqrt{2}} \frac{1}{\Lambda^2} \text{Re}\,[\mathcal{C}'_{\substack{e\gamma \\ \mu\mu}}], \tag{71}$$

where $v \approx 246$ GeV. Let us input the value

$$\Delta a_\mu = 249 \times 10^{-11}, \tag{72}$$

then, we obtain the Wilson coefficient as:

$$\frac{1}{\Lambda^2} \text{Re}\,[\mathcal{C}'_{\substack{e\gamma \\ \mu\mu}}] = 1.0 \times 10^{-5}\,\text{TeV}^{-2}, \tag{73}$$

where $e \simeq 0.3028$ is put in the natural unit.

The tree-level expression of a radiative LFV rate in terms of the Wilson coefficients is

$$\mathcal{B}(\ell_r \to \ell_s \gamma) = \frac{m_{\ell_r}^3 v^2}{8\pi \Gamma_{\ell_r}} \frac{1}{\Lambda^4}\left(|\mathcal{C}'_{\substack{e\gamma \\ rs}}|^2 + |\mathcal{C}'_{\substack{e\gamma \\ sr}}|^2\right). \tag{74}$$

Taking the experimental bound $\mathcal{B}(\mu^+ \to e^+\gamma) < 3.1 \times 10^{-13}$ (90% C.L.) obtained by the combination of data from

MEG and MEG II experiments [26,27] in Eq. (20), we obtain the upper-bound of the Wilson coefficient as:

$$\frac{1}{\Lambda^2}|\mathcal{C}'_{\substack{e\gamma \\ e\mu(\mu e)}}| < 1.8\times 10^{-10}\,\text{TeV}^{-2}. \tag{75}$$

On the other hand, by taking the following experimental upper-bound of the branching ratios, $\mathcal{B}(\tau\to\mu+\gamma) < 4.2\times10^{-8}$ and $\mathcal{B}(\tau\to e\gamma) < 3.3\times10^{-8}$ [28,29], we obtain the upper-bound of the Wilson coefficient as:

$$\begin{aligned}\frac{1}{\Lambda^2}|\mathcal{C}'_{\substack{e\gamma \\ \mu\tau(\tau\mu)}}| &< 2.65\times 10^{-6}\,\text{TeV}^{-2},\\ \frac{1}{\Lambda^2}|\mathcal{C}'_{\substack{e\gamma \\ e\tau(\tau e)}}| &< 2.35\times 10^{-6}\,\text{TeV}^{-2},\end{aligned} \tag{76}$$

respectively.

C U_{L1} and U_{R1} in Model I

We discuss the charged lepton mass matrix in Model I:

$$\text{I}: \quad M_E \simeq v_d \begin{pmatrix} A_1 & X_1 p' & 0 \\ Y_1 p' & B_1 & 0 \\ 0 & 0 & \gamma_1 \end{pmatrix}_{RL}, \tag{77}$$

where

$$\begin{aligned} A_1 &= -\tilde{\alpha}_1(1-144\epsilon p) \simeq -\tilde{\alpha}_1\\ B_1 &= -\tilde{\beta}_1(1+24\epsilon p) \simeq -\tilde{\beta}_1,\\ X_1 &= 16\sqrt{3}\tilde{\alpha}_1\sqrt{\epsilon}, \qquad Y_1 = 8\sqrt{3}\tilde{\beta}_1\sqrt{\epsilon}. \end{aligned} \tag{78}$$

It is written as:

$$M_E \simeq v_d \begin{pmatrix} -\tilde{\alpha}_1 & X_1 e^{i\pi\tau_R} & 0 \\ Y_1 e^{i\pi\tau_R} & -\tilde{\beta}_1 & 0 \\ 0 & 0 & \gamma_1 \end{pmatrix}, \tag{79}$$

where $\tau_R \equiv \text{Re}\,\tau$, and $\mathcal{O}(\epsilon)$ is neglected. Then, we have

$$M_E^\dagger M_E \simeq v_d^2 \begin{pmatrix} \tilde{\alpha}_1^2+Y_1^2 & Z_{L1} & 0 \\ Z_{L1}^* & \tilde{\beta}_1^2+X_1^2 & 0 \\ 0 & 0 & \gamma_1^2 \end{pmatrix}. \tag{80}$$

Taking $\tilde{\alpha}_1 \ll \tilde{\beta}_1$, we have

$$\begin{aligned} Z_{L1} &\simeq -8\sqrt{3}\tilde{\beta}_1^2\sqrt{\epsilon}\left(1+2\frac{\tilde{\alpha}_1^2}{\tilde{\beta}_1^2}e^{2i\pi\tau_R}\right)e^{-i\pi\tau_R}\\ &\simeq -8\sqrt{3}\tilde{\beta}_1^2\sqrt{\epsilon}\left(1+2\frac{\tilde{\alpha}_1^2}{\tilde{\beta}_1^2}\cos 2\pi\tau_R\right)e^{-i\pi\tau_R}e^{i\phi_{L1}}, \end{aligned} \tag{81}$$

where

$$\phi_{L1} \simeq 2\frac{\tilde{\alpha}_1^2}{\tilde{\beta}_1^2}\sin 2\pi\tau_R. \tag{82}$$

By using phase matrix P_{L1}, it is rewritten as:

$$M_E^\dagger M_E \simeq v_d^2 P_{L1}\begin{pmatrix} \tilde{\alpha}_1^2 & -|Z_{L1}| & 0 \\ -|Z_{L1}| & \tilde{\beta}_1^2 & 0 \\ 0 & 0 & \gamma_1^2 \end{pmatrix} P_{L1}^*, \tag{83}$$

$$P_{L1} = \begin{pmatrix} 1 & 0 & 0 \\ 0 & e^{i(\pi\tau_R-\phi_{L1})} & 0 \\ 0 & 0 & 1 \end{pmatrix}, \tag{84}$$

where

$$|Z_{L1}| = 8\sqrt{3}\tilde{\beta}_1^2\sqrt{\epsilon}\left(1+2\frac{\tilde{\alpha}_1^2}{\tilde{\beta}_1^2}\cos 2\pi\tau_R\right). \tag{85}$$

The diagonal form of $M_E^\dagger M_E$ is obtained by using the following orthogonal matrix U_{L1} as $U_{L1}^T(P_{L1}^* M_E^\dagger M_E P_{L1})U_{L1}$:

$$U_{L1} = \begin{pmatrix} \cos\theta_{L1} & \sin\theta_{L1} & 0 \\ -\sin\theta_{L1} & \cos\theta_{L1} & 0 \\ 0 & 0 & 1 \end{pmatrix} \simeq \begin{pmatrix} 1 & \theta_{L1} & 0 \\ -\theta_{L1} & 1 & 0 \\ 0 & 0 & 1 \end{pmatrix}, \tag{86}$$

where

$$\begin{aligned} \tan 2\theta_{L1} &= \frac{-2|Z_{L1}|}{\tilde{\beta}_1^2-\tilde{\alpha}_1^2} \sim -\frac{2|Z_{L1}|}{\tilde{\beta}_1^2}\left(1-\frac{\tilde{\alpha}_1^2}{\tilde{\beta}_1^2}\right)^{-1}\\ &\quad -16\sqrt{3}\sqrt{\epsilon}\left[1+\frac{\tilde{\alpha}_1^2}{\tilde{\beta}_1^2}(1+2\cos 2\pi\tau_R)\right]. \end{aligned} \tag{87}$$

Then, we have

$$\theta_{L1} \simeq -8\sqrt{3}\sqrt{\epsilon}\left[1+\frac{\tilde{\alpha}_1^2}{\tilde{\beta}_1^2}(1+2\cos 2\pi\tau_R)\right]. \tag{88}$$

Let us discuss $M_E M_E^\dagger$ to obtain the right-handed mixing:

$$M_E M_E^\dagger \simeq v_d^2 \begin{pmatrix} \tilde{\alpha}_1^2+X_1^2 & Z_{R1} & 0 \\ Z_{R1}^* & \tilde{\beta}_1^2+Y_1^2 & 0 \\ 0 & 0 & \gamma_1^2 \end{pmatrix}_{RR}, \tag{89}$$

where

$$\begin{aligned} Z_{R1} &= -\tilde{\alpha}_1 Y_1 e^{-i\pi\tau_R} - \tilde{\beta}_1 X_1 e^{i\pi\tau_R}\\ &= -8\sqrt{3}\tilde{\alpha}_1\tilde{\beta}_1\sqrt{\epsilon}(e^{-i\pi\tau_R}+2e^{i\pi\tau_R})\\ &= -8\sqrt{3}\tilde{\alpha}_1\tilde{\beta}_1\sqrt{\epsilon}(3\cos\pi\tau_R + i\sin\pi\tau_R) \end{aligned}$$

$$= -8\sqrt{3}\tilde{\alpha}_1\tilde{\beta}_1\sqrt{\epsilon}\sqrt{5+4\cos 2\pi\tau_R}e^{i\phi_R}, \quad (90)$$

where

$$\tan\phi_R = \frac{1}{3}\tan\pi\tau_R. \quad (91)$$

By using the phase matrix P_R, we have

$$M_E M_E^\dagger \simeq v_d^2 P_{R1}\begin{pmatrix} \tilde{\alpha}_1^2+X_1^2 & -|Z_{1R}| & 0 \\ -|Z_{1R}| & \tilde{\beta}_1^2+Y_1^2 & 0 \\ 0 & 0 & \gamma_1^2 \end{pmatrix}_{RR} P_{R1}^*, \quad (92)$$

$$P_{R1} = \begin{pmatrix} 1 & 0 & 0 \\ 0 & e^{-i\phi_R} & 0 \\ 0 & 0 & 1 \end{pmatrix}. \quad (93)$$

The diagonal form of $M_E M_E^\dagger$ is obtained by using the following orthogonal matrix U_R as $U_{R1}^T(P_{R1}^* M_E M_E^\dagger P_{R1})U_{R1}$:

$$U_{R1} = \begin{pmatrix} \cos\theta_{R1} & \sin\theta_{R1} & 0 \\ -\sin\theta_{R1} & \cos\theta_{R1} & 0 \\ 0 & 0 & 1 \end{pmatrix} \simeq \begin{pmatrix} 1 & \theta_{R1} & 0 \\ -\theta_{R1} & 1 & 0 \\ 0 & 0 & 1 \end{pmatrix}, \quad (94)$$

where

$$\tan 2\theta_{R1} = \frac{-2|Z_{R1}|}{\tilde{\beta}_1^2-\tilde{\alpha}_1^2} \simeq -\frac{2|Z_{R1}|}{\tilde{\beta}_1^2} \simeq -16\sqrt{3}\sqrt{\epsilon}\frac{\tilde{\alpha}_1}{\tilde{\beta}_1}\sqrt{5+4\cos 2\pi\tau_R}. \quad (95)$$

Finally, we get

$$\theta_{R1} \simeq -8\sqrt{3}\sqrt{\epsilon}\frac{\tilde{\alpha}_1}{\tilde{\beta}_1}\sqrt{5+4\cos 2\pi\tau_R}. \quad (96)$$

In order to obtain the approximate diagonal mass matrix from Eq. (79) by using the mixing angles of Eqs. (88), (96) and phase matrix P_{L1} of Eq. (84), P_{R1} of Eq. (93), we calculate $U_{R1}^T P_{R1}^* M_E P_{L1} U_{L1}$. Then we obtain the diagonal matrix elements up to $\mathcal{O}(\sqrt{\epsilon})$ as follows:

$$\begin{aligned} &M_E(1,1) \simeq -\tilde{\alpha}_1, \quad M_E(2,2) \simeq -\tilde{\beta}_1, \quad M_E(3,3) = \gamma_1, \\ &M_E(1,2) \simeq 8\sqrt{3}\tilde{\alpha}_1\sqrt{\epsilon}e^{-i(\phi_R+\pi\tau_R)} \\ &\left[1+2e^{2i\pi\tau_R}-e^{i(\phi_R+\pi\tau_R)}\sqrt{5+4\cos 2\pi\tau_R}\right] = 0, \\ &M_E(2,1) \simeq 8\sqrt{3}\tilde{\alpha}_1\frac{\tilde{\alpha}_1}{\tilde{\beta}_1}\sqrt{\epsilon} \\ &\left[-(1+2e^{-2i\pi\tau_R})e^{i(\phi_R+\pi\tau_R)}+\sqrt{5+4\cos 2\pi\tau_R}\right] = 0, \\ &M_E(1,3) = M_E(3,1) = M_E(2,3) = M_E(3,2) = 0, \end{aligned} \quad (97)$$

where the phases of diagonal matrix elements are removed by the redefinition of charged lepton fields. In $M_E(1,2)$ and $M_E(2,1)$, we have used following equations:

$$\begin{aligned} &\tan\phi_R = \frac{1}{3}\tan\pi\tau_R, \\ &1+2e^{2i\pi\tau_R} = \sqrt{5+4\cos 2\pi\tau_R}\, e^{i(\phi_R+\pi\tau_R)}. \end{aligned} \quad (98)$$

D U_{L2} and U_{R2} in Model II

We discuss the charged leptom mass matrix in Model II :

$$\text{II}: \quad M_E \simeq v_d\begin{pmatrix} A_2 & X_2 p' & F_2 p' \\ Y_2 p' & B_2 & 0 \\ 0 & 0 & \gamma_2 \end{pmatrix}_{RL}, \quad (99)$$

where

$$\begin{aligned} &A_2 = \tilde{\alpha}_2(1+264\epsilon p) \simeq \tilde{\alpha}_2, \\ &B_2 = -\tilde{\beta}_2(1+24\epsilon p) \simeq -\tilde{\beta}_2, \\ &X_2 = 8\sqrt{3}\tilde{\alpha}_2\sqrt{\epsilon}, \quad Y_2 = 8\sqrt{3}\tilde{\beta}_2\sqrt{\epsilon}, \\ &F_2 = -24\sqrt{3}\tilde{\alpha}_D\sqrt{\epsilon}. \end{aligned} \quad (100)$$

It is written as:

$$M_E \simeq v_d\begin{pmatrix} \tilde{\alpha}_2 & X_2 e^{i\pi\tau_R} & F_2 e^{i\pi\tau_R} \\ Y_2 e^{i\pi\tau_R} & -\tilde{\beta}_2 & 0 \\ 0 & 0 & \gamma_2 \end{pmatrix}, \quad (101)$$

where $\tau_R \equiv \mathrm{Re}\,\tau$. Then, we have

$$M_E^\dagger M_E \simeq v_d^2\begin{pmatrix} \tilde{\alpha}_2^2+Y_2^2 & Z_{L2} & \tilde{\alpha}_2 F_2 e^{i\pi\tau_R} \\ Z_{L2}^* & \tilde{\beta}_2^2+X_2^2 & X_2 F_2 \\ \tilde{\alpha}_2 F_2 e^{-i\pi\tau_R} & X_2 F_2 & \gamma_2^2 \end{pmatrix}, \quad (102)$$

where

$$\begin{aligned} Z_{L2} &= -8\sqrt{3}\tilde{\beta}_2^2\sqrt{\epsilon}e^{-i\pi\tau_R}\left(1-\frac{\tilde{\alpha}_2^2}{\tilde{\beta}_2^2}e^{2i\pi\tau_R}\right) \\ &\simeq -8\sqrt{3}\tilde{\beta}_2^2\sqrt{\epsilon}e^{-i\pi\tau_R}e^{i\phi_{L2}}\left|1-\frac{\tilde{\alpha}_2^2}{\tilde{\beta}_2^2}e^{2i\pi\tau_R}\right| \\ &\simeq -8\sqrt{3}\tilde{\beta}_2^2\sqrt{\epsilon}e^{-i\pi\tau_R}e^{i\phi_{L2}}\left(1-\frac{\tilde{\alpha}_2^2}{\tilde{\beta}_2^2}\cos 2\pi\tau_R\right), \end{aligned} \quad (103)$$

and

$$\phi_{L2} \simeq -\frac{\tilde{\alpha}_2^2}{\tilde{\beta}_2^2}\sin 2\pi\tau_R. \quad (104)$$

Up to $\mathcal{O}(\sqrt{\epsilon})$, we have

$$M_E^\dagger M_E \simeq v_d^2 \begin{pmatrix} \tilde{\alpha}_2^2 & -|Z_{L2}|e^{-i(\pi\tau_R-\phi_{L2})} & \tilde{\alpha}_2 F_2\, e^{i\pi\tau_R} \\ -|Z_{L2}|e^{i(\pi\tau_R-\phi_{L2})} & \tilde{\beta}_2^2 & X_2 F_2 \\ \tilde{\alpha}_2 F_2\, e^{-i\pi\tau_R} & X_2 F_2 & \gamma_2^2 \end{pmatrix}, \tag{105}$$

where the (2,3) and (3,2) entries are $\mathcal{O}(\epsilon)$. By using phase matrix P_{L2}, it is rewritten as:

$$M_E^\dagger M_E \simeq v_d^2\, P_{2L} \begin{pmatrix} \tilde{\alpha}_1^2 & -|Z_{L2}| & -24\sqrt{3}\tilde{\alpha}_2\tilde{\alpha}_D\sqrt{\epsilon} \\ -|Z_{L2}| & \tilde{\beta}_2^2 & -576\,\tilde{\alpha}_2\tilde{\alpha}_D\,\epsilon\, e^{-i(2\pi\tau_R-\phi_{L2})} \\ -24\sqrt{3}\tilde{\alpha}_2\tilde{\alpha}_D\sqrt{\epsilon} & -576\,\tilde{\alpha}_2\tilde{\alpha}_D\,\epsilon\, e^{i(2\pi\tau_R-\phi_{L2})} & \gamma_2^2 \end{pmatrix} P_{2L}^*, \tag{106}$$

where

$$P_{L2} = \begin{pmatrix} 1 & 0 & 0 \\ 0 & e^{i(\pi\tau_R-\phi_{L2})} & 0 \\ 0 & 0 & e^{-i\pi\tau_R} \end{pmatrix}, \tag{107}$$

and

$$|Z_{L2}| \simeq 8\sqrt{3}\tilde{\beta}_2^2\sqrt{\epsilon}\left(1-\frac{\tilde{\alpha}_2^2}{\tilde{\beta}_2^2}\cos 2\pi\tau_R\right). \tag{108}$$

The diagonal form of $M_E^\dagger M_E$ is obtained by using the following unitary matrix U_{L2} as $U_{L2}^\dagger(P_{L2}^* M_E^\dagger M_E P_{L2})U_{L2}$. Since (1,3), (3,1), (2,3) and (3,2) elements of $M_E^\dagger M_E$ is much smaller than $\tilde{\beta}_2^2$ and $|Z_{L2}|$, it is given approximately:

$$U_{L2} \simeq \begin{pmatrix} \cos\theta_{L2} & \sin\theta_{L2} & \theta_{L13} \\ -\sin\theta_{L2} & \cos\theta_{L2} & V_{L23} \\ -\theta_{L13} & -V_{L23}^* & 1 \end{pmatrix} \simeq \begin{pmatrix} 1 & \theta_{L2} & \theta_{L13} \\ -\theta_{L2} & 1 & V_{L23} \\ -\theta_{L13} & -V_{L23}^* & 1 \end{pmatrix}, \tag{109}$$

where

$$\tan 2\theta_{L2} = \frac{-2|Z_{L2}|}{\tilde{\beta}_2^2-\tilde{\alpha}_2^2} \simeq -\frac{2|Z_{L2}|}{\tilde{\beta}_2^2}\left(1-\frac{\tilde{\alpha}_2^2}{\tilde{\beta}_2^2}\right)^{-1} \simeq -16\sqrt{3}\sqrt{\epsilon}\left[1+\frac{\tilde{\alpha}_2^2}{\tilde{\beta}_2^2}\left(1-\cos 2\pi\tau_R\right)\right]. \tag{110}$$

Then, we have

$$\theta_{L2} \simeq -8\sqrt{3}\sqrt{\epsilon}\left[1+\frac{\tilde{\alpha}_2^2}{\tilde{\beta}_2^2}\left(1-\cos 2\pi\tau_R\right)\right]. \tag{111}$$

On the other hand, we have

$$\theta_{L13} \simeq -\frac{24\sqrt{3}\tilde{\alpha}_2\tilde{\alpha}_D}{\gamma_2^2}\sqrt{\epsilon}, \quad V_{L23} \simeq \frac{576\tilde{\alpha}_2\tilde{\alpha}_D}{\gamma_2^2}\epsilon\left[1-e^{i(\phi_{L2}-2\pi\tau_R)}\right]. \tag{112}$$

Let us discuss $M_E M_E^\dagger$ to obtain the right-handed mixing:

$$M_E M_E^\dagger \simeq v_d^2 \begin{pmatrix} \tilde{\alpha}_2^2+X_2^2+F_2^2 & Z_{R2} & F_2\gamma_2 p' \\ Z_{R1}^* & \tilde{\beta}_2^2+Y_2^2 & 0 \\ F_2\gamma_2 p'^* & 0 & \gamma_2^2 \end{pmatrix}_{RR}, \tag{113}$$

where

$$Z_{R2} = \tilde{\alpha}_2 Y_2 e^{-i\pi\tau_R} - \tilde{\beta}_2 X_2 e^{i\pi\tau_R} = 8\sqrt{3}\tilde{\alpha}_2\tilde{\beta}_2\sqrt{\epsilon}(e^{-i\pi\tau_R}-e^{i\pi\tau_R}) = -16i\sqrt{3}\tilde{\alpha}_2\tilde{\beta}_2\sqrt{\epsilon}\sin\pi\tau_R. \tag{114}$$

By using the phase matrix P_{2R}, we have

$$M_E M_E^\dagger \simeq v_d^2 P_{R2} \begin{pmatrix} \tilde{\alpha}_2^2(1+192\epsilon) & -|Z_{R2}| & -24\sqrt{3}\tilde{\alpha}_D\gamma_2\sqrt{\epsilon} \\ -|Z_{R2}| & \tilde{\beta}_2^2(1+192\epsilon) & 0 \\ -24\sqrt{3}\tilde{\alpha}_D\gamma_2\sqrt{\epsilon} & 0 & \gamma_2^2 \end{pmatrix}_{RR} P_{R2}^*, \tag{115}$$

where

$$P_{R2} = \begin{pmatrix} 1 & 0 & 0 \\ 0 & -i & 0 \\ 0 & 0 & e^{-i\pi\tau_R} \end{pmatrix}, \tag{116}$$

and

$$|Z_{R2}| = 16\sqrt{3}\tilde{\alpha}_2\tilde{\beta}_2\sqrt{\epsilon}\sin\pi\tau_R. \tag{117}$$

The diagonal form of $M_E M_E^\dagger$ is obtained by using the following orthogonal matrix U_{R2} as $U_{R2}^T(P_{R2}^* M_E M_E^\dagger P_{R2})U_{R2}$:

$$U_{R2} \simeq \begin{pmatrix} \cos\theta_{R2} & \sin\theta_{R2} & \theta_{R13} \\ -\sin\theta_{R2} & \cos\theta_{R2} & 0 \\ -\theta_{R13} & 0 & 1 \end{pmatrix} \simeq \begin{pmatrix} 1 & \theta_{R2} & \theta_{R13} \\ -\theta_{R2} & 1 & 0 \\ -\theta_{R13} & 0 & 1 \end{pmatrix}, \tag{118}$$

where

$$\tan 2\theta_{R2} = \frac{-2|Z_{R2}|}{\tilde{\beta}_2^2 - \tilde{\alpha}_2^2} \simeq -\frac{2|Z_{R2}|}{\tilde{\beta}_2^2} \simeq -32\sqrt{3}\sqrt{\epsilon}\frac{\tilde{\alpha}_2}{\tilde{\beta}_2}\sin\pi\tau_R. \tag{119}$$

Therefore, we get approximately

$$\theta_{R2} \simeq -16\sqrt{3}\sqrt{\epsilon}\frac{\tilde{\alpha}_2}{\tilde{\beta}_2}\sin\pi\tau_R. \tag{120}$$

On the other hand, we have

$$\theta_{R13} \simeq -24\sqrt{3}\frac{\tilde{\alpha}_D}{\gamma_2}\sqrt{\epsilon}. \tag{121}$$

In order to obtain the approximate diagonal mass matrix from Eq. (101) by using the mixing angles of Eqs. (111), (120) and phase matrix P_{L2} of Eq. (107), P_{R2} of Eq. (116), we calculate $U_{R2}^T P_{R2}^* M_E P_{L2} U_{L2}$. Then we obtain the approximate mass matrix elements up to $\mathcal{O}(\sqrt{\epsilon})$ as follows:

$$\begin{aligned}
&M_E(1,1) \simeq \tilde{\alpha}_2, \qquad M_E(2,2) \simeq -\tilde{\beta}_2, \qquad M_E(3,3) \simeq \gamma_2,\\
&M_E(1,2) \simeq 8\sqrt{3}\tilde{\alpha}_2\sqrt{\epsilon}\, i e^{-i\pi\tau_R}\\
&\quad\left(-1 + e^{2i\pi\tau_R} - 2i\, e^{i\pi\tau_R}\sin\pi\tau_R\right) = 0,\\
&M_E(2,1) \simeq 8\, i\, e^{i\pi\tau_R}\sqrt{3}\tilde{\alpha}_2\frac{\tilde{\alpha}_2}{\tilde{\beta}_2}\\
&\sqrt{\epsilon}(e^{-2i\pi\tau_R} - 1 + 2i\sin\pi\tau_R e^{-i\pi\tau_R}) = 0,\\
&M_E(1,3) \simeq -24\sqrt{3}\tilde{\alpha}_2\frac{\tilde{\alpha}_2\tilde{\alpha}_D}{\gamma_2^2}\sqrt{\epsilon},\\
&M_E(3,1) \simeq -4608\sqrt{3}\tilde{\alpha}_2\frac{\tilde{\alpha}_D}{\gamma_2}\epsilon\sqrt{\epsilon}e^{2i\pi\tau_R},\\
&M_E(2,3) \sim \tilde{\alpha}_2\,\mathcal{O}\left(\frac{\tilde{\alpha}_D}{\tilde{\beta}_2}\epsilon\right),\\
&M_E(3,2) \sim \tilde{\alpha}_2\,\mathcal{O}\left(\frac{\tilde{\alpha}_D}{\gamma_2}\frac{\tilde{\alpha}_2^2}{\tilde{\beta}_2^2}\epsilon\right),
\end{aligned} \tag{122}$$

where the phases of diagonal matrix elements are removed by the redefinition of charged lepton fields. In $M_E(1,2)$ and $M_E(2,1)$, we have used the identity:

$$1 - e^{2i\pi\tau_R} = -2i\, e^{i\pi\tau_R}\sin\pi\tau_R. \tag{123}$$

E Model parameters in Normal distribution

In our analyses, we scatter the parameters δ_α, δ_β, δ_γ and δ_D in the normal distribution with an average 0 and the standard deviation σ in Eq. (53)

$$F = F_0 \exp\left(-\frac{x^2}{2\sigma^2}\right), \tag{124}$$

where F_0 is a normalization constant. Since the mean square of x is $\langle x^2\rangle = \sigma^2$, we have

$$\sqrt{\langle\delta_\alpha^2\rangle} = \sqrt{\langle\delta_\beta^2\rangle} = \sqrt{\langle\delta_\gamma^2\rangle} = \sqrt{\langle\delta_D^2\rangle} = \sigma. \tag{125}$$

In our statistical discussions, we take

$$\begin{aligned}
&|\delta_\alpha| \simeq \sqrt{\langle\delta_\alpha^2\rangle}, \quad |\delta_\beta| \simeq \sqrt{\langle\delta_\beta^2\rangle},\\
&|\delta_\gamma| \simeq \sqrt{\langle\delta_\gamma^2\rangle}, \quad |\delta_D| \simeq \sqrt{\langle\delta_D^2\rangle}.
\end{aligned} \tag{126}$$

Therefore, we obtain the relevant factors as:

$$\left|1 - \frac{\alpha_{1(2)}}{\alpha'_{1(2)}}\frac{\beta'_{1(2)}}{\beta_{1(2)}}\right| \simeq \sigma, \quad \left|1 - \frac{\alpha_D}{\alpha'_D}\frac{\gamma'_2}{\gamma_2}\right| \simeq \sigma, \tag{127}$$

which appear in the coefficients of Eqs. (49) and (52).

References

1. D.P. Aguillard et al. [Muon g-2], Phys. Rev. Lett. **131**(16), 161802 (2023). arXiv:2308.06230 [hep-ex]
2. B. Abi et al. [Muon g-2], Phys. Rev. Lett. **126**(14), 141801 (2021). arXiv:2104.03281 [hep-ex]
3. G.W. Bennett et al. [Muon g-2], Phys. Rev. D **73**, 072003 (2006). arXiv:hep-ex/0602035 [hep-ex]
4. T. Aoyama, N. Asmussen, M. Benayoun, J. Bijnens, T. Blum, M. Bruno, I. Caprini, C.M. Carloni Calame, M. Cè, G. Colangelo et al., Phys. Rep. **887**, 1–166 (2020). arXiv:2006.04822 [hep-ph]
5. F. Jegerlehner, Springer Tracts Mod. Phys. **274**, 1–693 (2017)
6. G. Colangelo, M. Hoferichter, P. Stoffer, JHEP **02**, 006 (2019). arXiv:1810.00007 [hep-ph]
7. M. Hoferichter, B.L. Hoid, B. Kubis, JHEP **08**, 137 (2019). arXiv:1907.01556 [hep-ph]
8. M. Davier, A. Hoecker, B. Malaescu, Z. Zhang, Eur. Phys. J. C **80**(3), 241 (2020). [Erratum: Eur. Phys. J. C **80** (2020) no.5, 410]. arXiv:1908.00921 [hep-ph]
9. A. Keshavarzi, D. Nomura, T. Teubner, Phys. Rev. D **101**(1), 014029 (2020). arXiv:1911.00367 [hep-ph]
10. B.L. Hoid, M. Hoferichter, B. Kubis, Eur. Phys. J. C **80**(10), 988 (2020). arXiv:2007.12696 [hep-ph]
11. A. Czarnecki, W.J. Marciano, A. Vainshtein, Phys. Rev. D **67**, 073006 (2003). [Erratum: Phys. Rev. D **73** (2006), 119901]. arXiv:hep-ph/0212229 [hep-ph]
12. K. Melnikov, A. Vainshtein, Phys. Rev. D **70**, 113006 (2004). arXiv:hep-ph/0312226 [hep-ph]
13. T. Aoyama, M. Hayakawa, T. Kinoshita, M. Nio, Phys. Rev. Lett. **109**, 111808 (2012). arXiv:1205.5370 [hep-ph]
14. C. Gnendiger, D. Stöckinger, H. Stöckinger-Kim, Phys. Rev. D **88**, 053005 (2013). arXiv:1306.5546 [hep-ph]
15. F.V. Ignatov et al. [CMD-3], Phys. Rev. D **109**(11), 112002 (2024). arXiv:2302.08834 [hep-ex]
16. I. Adachi et al. [Belle-II], arXiv:2404.04915 [hep-ex]
17. S. Borsanyi, Z. Fodor, J.N. Guenther, C. Hoelbling, S.D. Katz, L. Lellouch, T. Lippert, K. Miura, L. Parato, K.K. Szabo et al., Nature **593**(7857), 51–55 (2021). arXiv:2002.12347 [hep-lat]
18. T.S. Roussy, L. Caldwell, T. Wright, W.B. Cairncross, Y. Shagam, K.B. Ng, N. Schlossberger, S.Y. Park, A. Wang, J. Ye et al., Science **381**(6653), adg4084 (2023). arXiv:2212.11841 [physics.atom-ph]
19. V. Andreev et al. [ACME], Nature **562**(7727), 355–360 (2018)

20. D.M. Kara, I.J. Smallman, J.J. Hudson, B.E. Sauer, M.R. Tarbutt, E.A. Hinds, New J. Phys. **14**, 103051 (2012). arXiv:1208.4507 [physics.atom-ph]
21. J. Doyle, Search for the Electric Dipole Moment of the Electron with Thorium Monoxide—The ACME Experiment. Talk at the KITP (2016)
22. G.W. Bennett et al. [Muon (g-2)], Phys. Rev. D **80**, 052008 (2009). arXiv:0811.1207 [hep-ex]
23. K. Inami et al. [Belle], Phys. Lett. B **551**, 16–26 (2003). arXiv:hep-ex/0210066 [hep-ex]
24. W. Bernreuther, L. Chen, O. Nachtmann, Phys. Rev. D **103**(9), 096011 (2021). arXiv:2101.08071 [hep-ph]
25. K. Uno, PoS ICHEP2022, 721 (2022)
26. A.M. Baldini et al. [MEG], Eur. Phys. J. C **76**(8), 434 (2016). arXiv:1605.05081 [hep-ex]
27. K. Afanaciev et al. [MEG II], Eur. Phys. J. C **84**(3), 216 (2024). arXiv:2310.12614 [hep-ex]
28. B. Aubert et al. [BaBar], Phys. Rev. Lett. **104**, 021802 (2010). arXiv:0908.2381 [hep-ex]
29. A. Abdesselam et al. [Belle], JHEP **10**, 19 (2021). arXiv:2103.12994 [hep-ex]
30. W. Buchmuller, D. Wyler, Nucl. Phys. B **268**, 621–653 (1986)
31. B. Grzadkowski, M. Iskrzynski, M. Misiak, J. Rosiek, JHEP **10**, 085 (2010). arXiv:1008.4884 [hep-ph]
32. R. Alonso, E.E. Jenkins, A.V. Manohar, M. Trott, JHEP **04**, 159 (2014). arXiv:1312.2014 [hep-ph]
33. G. Panico, A. Pomarol, M. Riembau, JHEP **04**, 090 (2019). arXiv:1810.09413 [hep-ph]
34. J. Aebischer, W. Dekens, E.E. Jenkins, A.V. Manohar, D. Sengupta, P. Stoffer, JHEP **07**, 107 (2021). arXiv:2102.08954 [hep-ph]
35. L. Allwicher, P. Arnan, D. Barducci, M. Nardecchia, JHEP **10**, 129 (2021). arXiv:2108.00013 [hep-ph]
36. J. Kley, T. Theil, E. Venturini, A. Weiler, arXiv:2109.15085 [hep-ph]
37. G. Isidori, J. Pagès, F. Wilsch, JHEP **03**, 011 (2022). arXiv:2111.13724 [hep-ph]
38. M. Tanimoto, K. Yamamoto, Eur. Phys. J. C **84**(3), 252 (2024). arXiv:2310.16325 [hep-ph]
39. L. Calibbi, M.L. López-Ibáñez, A. Melis, O. Vives, Eur. Phys. J. C **81**(10), 929 (2021). arXiv:2104.03296 [hep-ph]
40. F. Feruglio, in *From My Vast Repertoire ...: Guido Altarelli's Legacy*, ed. by A. Levy, S. Forte, Stefano, G. Ridolfi, pp. 227–266 (2019). arXiv:1706.08749 [hep-ph]
41. T. Kobayashi, K. Tanaka, T.H. Tatsuishi, Phys. Rev. D **98**, 016004 (2018). arXiv:1803.10391
42. J.T. Penedo, S.T. Petcov, Nucl. Phys. B **939**, 292 (2019). arXiv:1806.11040
43. P.P. Novichkov, J.T. Penedo, S.T. Petcov, A.V. Titov, JHEP **04**, 174 (2019). arXiv:1812.02158 [hep-ph]
44. E. Ma, G. Rajasekaran, Phys. Rev. D **64**, 113012 (2001). arXiv:hep-ph/0106291
45. K.S. Babu, E. Ma, J.W.F. Valle, Phys. Lett. B **552**, 207 (2003). arXiv:hep-ph/0206292
46. G. Altarelli, F. Feruglio, Nucl. Phys. B **720**, 64 (2005). arXiv:hep-ph/0504165
47. G. Altarelli, F. Feruglio, Nucl. Phys. B **741**, 215 (2006). arXiv:hep-ph/0512103
48. Y. Shimizu, M. Tanimoto, A. Watanabe, Prog. Theor. Phys. **126**, 81 (2011). arXiv:1105.2929 [hep-ph]
49. S.T. Petcov, A.V. Titov, Phys. Rev. D **97**(11), 115045 (2018). arXiv:1804.00182 [hep-ph]
50. S.K. Kang, Y. Shimizu, K. Takagi, S. Takahashi, M. Tanimoto, PTEP **2018**(8), 083B01 (2018). arXiv:1804.10468 [hep-ph]
51. J.C. Criado, F. Feruglio, SciPost Phys. **5**, 042 (2018). arXiv:1807.01125 [hep-ph]
52. T. Kobayashi, N. Omoto, Y. Shimizu, K. Takagi, M. Tanimoto, T.H. Tatsuishi, JHEP **1811**, 196 (2018). arXiv:1808.03012 [hep-ph]
53. F.J. de Anda, S.F. King, E. Perdomo, Phys. Rev. D **101**(1), 015028 (2020). arXiv:1812.05620 [hep-ph]
54. P.P. Novichkov, S.T. Petcov, M. Tanimoto, Phys. Lett. B **793**, 247 (2019). arXiv:1812.11289 [hep-ph]
55. H. Okada, M. Tanimoto, Phys. Lett. B **791**, 54–61 (2019). arXiv:1812.09677 [hep-ph]
56. G.J. Ding, S.F. King, X.G. Liu, JHEP **1909**, 074 (2019). arXiv:1907.11714 [hep-ph]
57. H. Okada, M. Tanimoto, Eur. Phys. J. C **81**, 52 (2021). arXiv:1905.13421 [hep-ph]
58. H. Okada, M. Tanimoto, Phys. Dark Univ. **40**, 101204 (2023). arXiv:2005.00775 [hep-ph]
59. H. Okada, M. Tanimoto, Phys. Rev. D **103**, 015005 (2021). arXiv:2009.14242 [hep-ph]
60. H. Okada, M. Tanimoto, JHEP **03**, 010 (2021). arXiv:2012.01688 [hep-ph]
61. H. Okada, Y. Shimizu, M. Tanimoto, T. Yoshida, JHEP **07**, 184 (2021). arXiv:2105.14292 [hep-ph]
62. T. Kobayashi, H. Otsuka, M. Tanimoto, K. Yamamoto, Phys. Rev. D **105**, 055022 (2022). arXiv:2112.00493 [hep-ph]
63. T. Kobayashi, H. Otsuka, M. Tanimoto, K. Yamamoto, JHEP **08**, 013 (2022). arXiv:2204.12325 [hep-ph]
64. S.T. Petcov, M. Tanimoto, Eur. Phys. J. C **83**, 579 (2023). arXiv:2212.13336 [hep-ph]
65. S.T. Petcov, M. Tanimoto, JHEP **08**, 086 (2023). arXiv:2306.05730 [hep-ph]
66. P.P. Novichkov, J.T. Penedo, S.T. Petcov, A.V. Titov, JHEP **04**, 005 (2019). arXiv:1811.04933 [hep-ph]
67. X.G. Liu, G.J. Ding, JHEP **08**, 134 (2019). arXiv:1907.01488 [hep-ph]
68. P.P. Novichkov, J.T. Penedo, S.T. Petcov, Nucl. Phys. B **963**, 115301 (2021). arXiv:2006.03058 [hep-ph]
69. C.Y. Yao, X.G. Liu, G.J. Ding, Phys. Rev. D **103**, 095013 (2021). arXiv:2011.03501 [hep-ph]
70. G.J. Ding, F. Feruglio, X.G. Liu, SciPost Phys. **10**, 133 (2021). arXiv:2102.06716 [hep-ph]
71. P.P. Novichkov, J.T. Penedo, S.T. Petcov, JHEP **04**, 206 (2021). arXiv:2102.07488 [hep-ph]
72. G.J. Ding, S.F. King, C.Y. Yao, Phys. Rev. D **104**, 055034 (2021). arXiv:2103.16311 [hep-ph]
73. C.C. Li, X.G. Liu, G.J. Ding, JHEP **10**, 238 (2021). arXiv:2108.02181 [hep-ph]
74. I. de Medeiros Varzielas, M. Levy, J. T. Penedo, S. T. Petcov, JHEP **09**, 196 (2023). arXiv:2307.14410 [hep-ph]
75. G.J. Ding, X.G. Liu, J.N. Lu, M.H. Weng, JHEP **11**, 083 (2023). arXiv:2307.14926 [hep-ph]
76. D. Meloni, M. Parriciatu, JHEP **09**, 043 (2023). arXiv:2306.09028 [hep-ph]
77. S. Marciano, D. Meloni, M. Parriciatu, JHEP **05**, 020 (2024). arXiv:2402.18547 [hep-ph]
78. G. Altarelli, F. Feruglio, Rev. Mod. Phys. **82**, 2701 (2010). arXiv:1002.0211 [hep-ph]
79. H. Ishimori, T. Kobayashi, H. Ohki, Y. Shimizu, H. Okada, M. Tanimoto, Prog. Theor. Phys. Suppl. **183**, 1 (2010). arXiv:1003.3552 [hep-th]
80. H. Ishimori, T. Kobayashi, H. Ohki, H. Okada, Y. Shimizu, M. Tanimoto, Lect. Notes Phys. **858**, 1. Springer (2012)
81. T. Kobayashi, H. Ohki, H. Okada, Y. Shimizu, M. Tanimoto, Lect. Notes Phys. **995**, 1. Springer (2022)
82. D. Hernandez, A.Y. Smirnov, Phys. Rev. D **86**, 053014 (2012). arXiv:1204.0445 [hep-ph]
83. S.F. King, C. Luhn, Rep. Prog. Phys. **76**, 056201 (2013). arXiv:1301.1340 [hep-ph]

84. S.F. King, A. Merle, S. Morisi, Y. Shimizu, M. Tanimoto, New J. Phys. **16**, 045018 (2014). arXiv:1402.4271 [hep-ph]
85. M. Tanimoto, AIP Conf. Proc. **1666**, 120002 (2015)
86. S.F. King, Prog. Part. Nucl. Phys. **94**, 217 (2017). arXiv:1701.04413 [hep-ph]
87. S.T. Petcov, Eur. Phys. J. C **78**, 709 (2018). arXiv:1711.10806 [hep-ph]
88. F. Feruglio, A. Romanino, Rev. Mod. Phys. **93**(1), 015007 (2021). arXiv:1912.06028 [hep-ph]
89. T. Kobayashi, M. Tanimoto, arXiv:2307.03384 [hep-ph]
90. F. Feruglio, A. Strumia, A. Titov, JHEP **07**, 027 (2023). arXiv:2305.08908 [hep-ph]
91. T. Higaki, J. Kawamura, T. Kobayashi, JHEP **04**, 147 (2024). arXiv:2402.02071 [hep-ph]
92. S.T. Petcov, M. Tanimoto, arXiv:2404.00858 [hep-ph]
93. J.T. Penedo, S.T. Petcov, arXiv:2404.08032 [hep-ph]
94. F. Feruglio, M. Parriciatu, A. Strumia, A. Titov, arXiv:2406.01689 [hep-ph]
95. Y. Abe, T. Higaki, F. Kaneko, T. Kobayashi, H. Otsuka, JHEP **06**, 187 (2023). arXiv:2303.02947 [hep-ph]
96. G.J. Ding, S.Y. Jiang, W. Zhao, arXiv:2405.06497 [hep-ph]
97. S.F. King, X. Wang, arXiv:2405.08924 [hep-ph]
98. G.F. Casas, L.E. Ibáñez, arXiv:2407.12081 [hep-th]
99. B.Y. Qu, G.J. Ding, arXiv:2406.02527 [hep-ph]
100. S. Kikuchi, T. Kobayashi, K. Nasu, H. Otsuka, S. Takada, H. Uchida, PTEP **2022**(12), 123B02 (2022). arXiv:2203.14667 [hep-ph]
101. T. Kobayashi, H. Otsuka, Eur. Phys. J. C **82**(1), 25 (2022). arXiv:2108.02700 [hep-ph]
102. J. Fuentes-Martín, G. Isidori, J. Pagès, K. Yamamoto, Phys. Lett. B **800**, 135080 (2020). arXiv:1909.02519 [hep-ph]
103. D.A. Faroughy, G. Isidori, F. Wilsch, K. Yamamoto, JHEP **08**, 166 (2020). arXiv:2005.05366 [hep-ph]
104. D. Buttazzo, P. Paradisi, Phys. Rev. D **104**(7), 075021 (2021). arXiv:2012.02769 [hep-ph]
105. Y. Okada, K.I. Okumura, Y. Shimizu, Phys. Rev. D **61**, 094001 (2000). arXiv:hep-ph/9906446 [hep-ph]
106. G.F. Giudice, P. Paradisi, M. Passera, JHEP **11**, 113 (2012). arXiv:1208.6583 [hep-ph]
107. D. Hanneke, S. Fogwell, G. Gabrielse, Phys. Rev. Lett. **100**, 120801 (2008). arXiv:0801.1134 [physics.atom-ph]
108. R.H. Parker, C. Yu, W. Zhong, B. Estey, H. Müller, Science **360**, 191 (2018). arXiv:1812.04130 [physics.atom-ph]
109. L. Morel, Z. Yao, P. Cladé, S. Guellati-Khélifa, Nature **588**(7836), 61–65 (2020)